FUEL EFFICIENT ATTITUDE CONTROL OF SPACECRAFT

by

YUJI HANAWA

B.E., Waseda University

(1969)

SUBMITTED IN PARTIAL FULFILLMENT
OF THE REQUIREMENTS FOR THE
DEGREE OF MASTER OF SCIENCE

at the

MASSACHUSETTS INSTITUTE OF TECHNOLOGY

June, 1979

Signature of Author_____

Department of Aeronautics and Astronautics
May 18, 1979

Certified by_____

Thesis Supervisor

Accepted by_____

Chairman, Departmental Graduate Committee

FUEL EFFICIENT ATTITUDE CONTROL OF SPACECRAFT

by

Yuji Hanawa

Submitted to the Department of
Aeronautics and Astronautics on May 18, 1979
in partial fulfillment of the requirements for
the degree of Master of Science.

ABSTRACT

A real time optimal attitude control scheme for a spacecraft which maximizes the fuel efficiency and minimizes the power consumption and disturbances to the mission is studied in this research. A geosynchronous-all-thruster three-axes attitude stabilized satellite, which has highly accurate attitude holding requirements so that more sophisticated missions can be achieved, is considered here. This scheme uses the 'Separate-Bias' Kalman filter so as to estimate the solar pressure torque bias accurately enough to predict the soft-limit cycle trajectory effectively. The predicted trajectory is used to determine each thruster on/off timing to satisfy optimality in real-time. The simulation results showed the feasibility of this scheme for practical use without reservation.

Thesis Supervisor : Wallace E. Vander Velde

Title : Professor of Aeronautics and Astronautics

ACKNOWLEDGEMENT

The author wishes to express his sincere gratitude to Professor Wallace E. Vander Velde, who, as his thesis supervisor, has guided and encouraged the author patiently throughout the work. His invaluable instructions based on his deep and vast knowledge permitted the author to complete the thesis.

Thanks are extended to Professor Jansson who gave me the basics of control theory and Professor W. Widnall who lead the author to an appreciation of modern control theories.

Special thanks go to Mr. and Mrs. Mackenzie of Wayland, Mass. who offered an accomodation for my family during the last phase of the work and whose encouragement is gratefully appreciated.

Finally the author would like to express hearty thanks to his wife, Kazuyo, who, having a tiny baby, has given the considerably pains-taking support which will never be forgotten by him.

TABLE OF CONTENTS

CHAPTER 1

INTRODUCTION

One of the significant features which are required of a geo-synchronous satellite currently is increased sophistication in the missions such as higher capacity and multiple narrow-beam communication[1], highly precise sensing of the earth surface, etc. Associated with these missions, accuracy requirements for attitude control during the station keeping phase are considerably higher, and a three-axes attitude control system has been used to meet them. Furthermore, current technology gives us an intelligent sensor which improves accuracy tremendously. Typically there are two approaches to three-axes attitude stabilization: one uses momentum exchange devices and the other uses thrusters.
An all-thruster scheme is potentially preferable since there are no moving parts in it. M. H. Kaplan[2],[3] proposed an all-electric thruster control scheme which yields very small (much smaller than a chemical thruster) repeatable impulse bits at very high specific impulse; thus, soft limit cycles are possible. However, the all-thruster scheme requires much fuel and frequent thrustings especially when accurate attitude hold is required.
If we use the all-electric thruster scheme fuel consumption is less than for a chemical thruster, but the power consumption will be the more practical problem.

Any of these facts restrict the missions inevitable. Therefore, to minimize these effects one has to maximize the period of the soft-limit cycle.

The study presented here is a real time optimal attitude control scheme which aims at maximization of the soft-limit cycle period. This scheme assumes the spacecraft to be a rigid body, and along with the attitude error states it estimates the solar pressure torque which is the dominant disturbance torque. It varies slowly with a period of 24 hours as the torque center rotates at orbital period. Once the solar pressure torque is given, one can predict the new trajectory of the limit-cycle from current estimated states. Then a real time control law can be constructed to achieve the optimum trajectory. A Kalman filter is used to estimate these states.

Attitude error angle measurements taken by a set of optical sensors are input to the filter. Since we are dealing with very precise angles, then not only the measurement noises are important but the measurement biases are to be considered as well. This is true for the treatment of the thrusting torques too. Usually, these biases are augmented to the prime states so that they are estimated[4]; that means, the Kalman filter has to handle the state vector and matrices with larger dimensions. Especially in our problem, the dimension of the biases is larger than that of the prime states. However, augmentation makes the estimation less efficient in terms of accuracy and computational speed in general.

The control scheme proposed here uses the 'Separate-Bias' Kalman filter devised by B. Friedland[5],[6] which deals with the bias states separately from the prime states so that the numerical inaccuracies introduced by computations with large vectors and matrices can be avoided. When a current estimated state trajectory comes in a region where thrusting is needed so as not to violate the attitude error limit, the real time control law determines at each sampling instant whether it is the right time for the thruster to be fired (or terminated) based on the predicted trajectory. In this study, approximated linear dynamic equations of the spacecraft are used for trajectory prediction.

A simulation of a typical all-electric thruster three-axes attitude control spacecraft has been performed. The simulation revealed excellent estimation capability of the solar pressure torque bias which assured the feasibility of this control scheme for use in practice without reservation. The 'Separate-Bias' Kalman filter estimated six prime states — roll, pitch, yaw error angle and angle rates — and eight bias states — two solar pressure torque components, three thrust bias torque components and three measurement bias components. At each time when the control mode shifted from thrust-free mode to thrusting mode the sampling period changed from 25 seconds to 1 second and reinitializations of some states and error covariance matrix adjustments were made so that the Kalman Gains would not become insensitive.

Despite these discontinuities the estimation errors were sufficiently small that the real time control law could achieve a close approximation to the optimal trajectory. Although there still exist some practical problems to be solved before implementing this control scheme in an actual on-board computer, these results give us strong confidence that it is worthwhile to do so.

CHAPTER 2

THE MODEL OF THE PROBLEM

2.1 Spacecraft Dynamic Equations

The spacecraft under consideration is assumed to be in geosynchronous orbit and the attitude is stabilized by an all-electric thruster three-axis attitude control system during the station keeping phase. This type of spacecraft usually possesses an axis always pointing toward the earth to perform its required missions such as communication with ground stations, monitoring the surface of the earth by a vidicon camera or scanning spectrometer, etc. For the power source it has solar cell paddles which are sun-oriented; that is, their surface normals are always parallel to the sun line. The spacecraft configuration on orbit is shown in Fig. 2.1.

To define the dynamic equations the following assumptions are made. The first is the rigid body assumption; that is, there exist no internal moving parts and the solar cell paddles do not bend. Secondly, the body fixed frame (x, y, z) has its origin at the center of mass and the axes coincide with the principal axes. Actually, fuel sloshing and paddle rotation with respect to the main body with the period of 24 hours do occur; however, those effects are very small in the station keeping phase and they can be neglected in this problem.

The dynamic equations are described by Euler's moment equations[6] in the form of

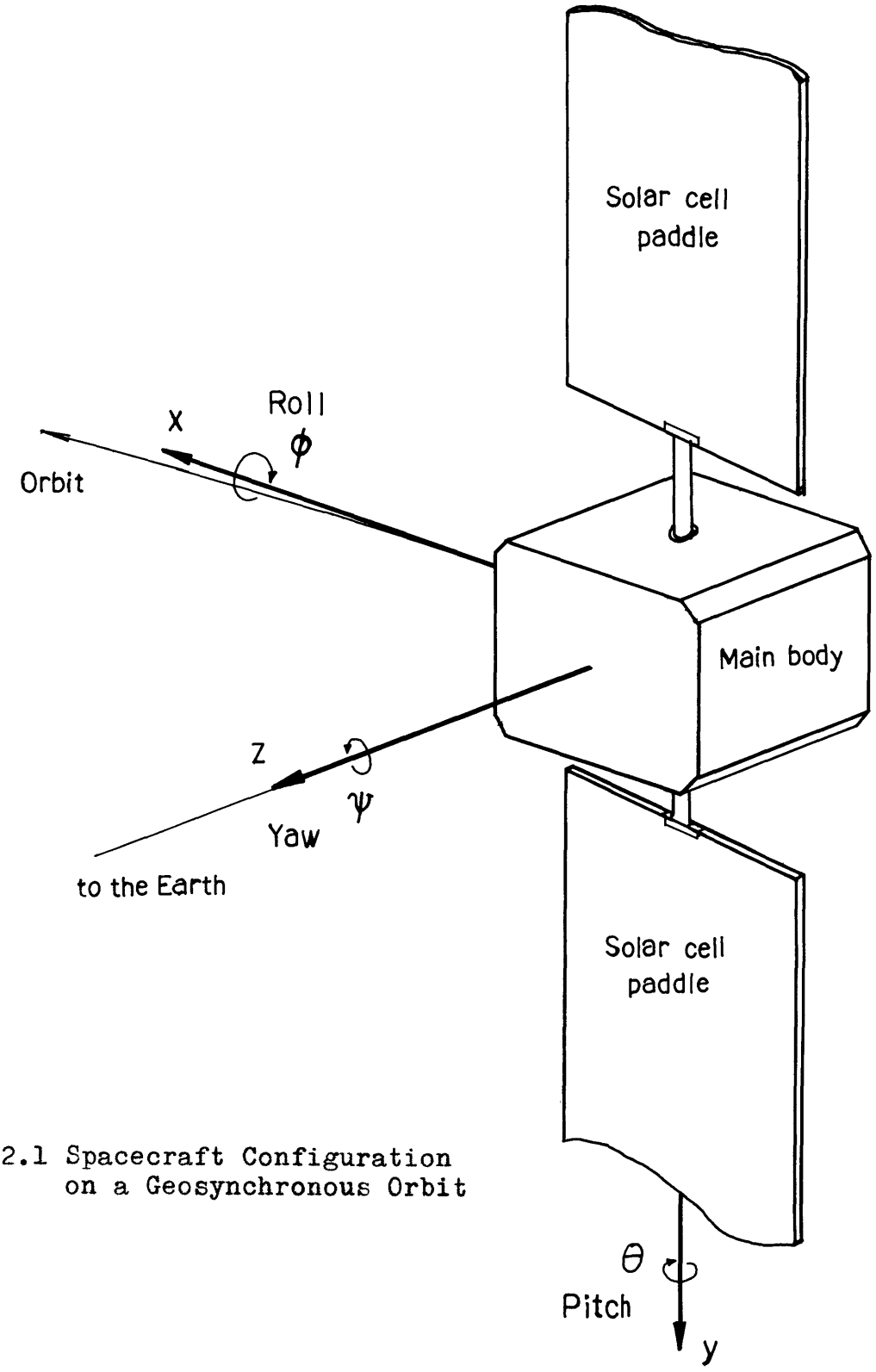

Fig.2.1 Spacecraft Configuration
on a Geosynchronous Orbit

$$Mx = Ix\dot{\omega}x + (Iz - Iy)\omega y\omega z \tag{2.1}$$

$$My = Iy\dot{\omega}y + (Ix - Iz)\omega x\omega z \tag{2.2}$$

$$Mz = Iz\dot{\omega}z + (Iy - Ix)\omega x\omega y \tag{2.3}$$

Where Mx, My and Mz are the body-fixed frame components of applied torque, Ix, Iy and Iz are the principal moments of inertia, and ωx, ωy and ωz are the angular velocity components.

2.2 External Torques

Two kinds of disturbance torques are considered here; solar pressure torque caused by the solar radiation interaction with the spacecraft surface, and gravitational torque.

The solar pressure torque creates a measurable deviation in the stabilized attitude that requires frequent attitude corrections. Generally, the center of the solar pressure and the direction and magnitude of the net pressure vector depend on a surface size, form and condition; incident angle of the sun line, the surface area, the reflectivity and absorptivity of the surface, etc. However, in our problem, the incident angle upon the solar cell paddles, which total area is dominant compared with that of the main body, is assumed to be 90 degrees, and usually the main body has a near cubic-shaped form which results in the fact that the torques produced by each side cancel each other. Therefore, we can neglect the torque due to the main body and that allows us to construct a simpler model. Also we assume that the sun line lies

in the xz-plane of the spacecraft which is an approximation to the actual situation. The geometrical relation of the solar cell paddles on orbit and the sun line is shown in Fig. 2.2.

Since the x, y, and z components of the net pressure vector $\underline{F}$ is expressed by

$$Fx = F_0 \cos w_0 t \tag{2.4}$$

$$Fy = 0 \tag{2.5}$$

$$Fz = -F_0 \sin w_0 t \tag{2.6}$$

where Fo is constant, then the solar pressure torque $\underline{S}$ can be defined by

$$Sx = -y_t F_0 \sin w_0 t \tag{2.7}$$

$$Sy = z_t F_0 \cos w_0 t + x_t F_0 \sin w_0 t \tag{2.8}$$

$$Sz = -y_t F_0 \cos w_0 t \tag{2.9}$$

where xt, yt, zt are the x, y, z components of the position vector $\underline{r}$t of the net pressure center, and wo, t are the angular velocity of the orbit and time respectively. It is reasonable to assume that $\underline{r}$t is nearly constant so that ytFo, ztFo and xtFo can be treated as constants.

Then Eq. (2.7), (2.8), (2.9) are rewritten in the form

$$Sx = - b_{sx} \sin w_0 t \tag{2.10}$$

$$Sy = b_{sy} \{\cos w_0 t + (\frac{xt}{zt}) \sin w_0 t\} \tag{2.11}$$

$$Sz = - b_{sz} \cos w_0 t \tag{2.12}$$

where

$$bsx = bsz = y_t Fo \tag{2.13}$$

$$bsy = z_t Fo \tag{2.14}$$

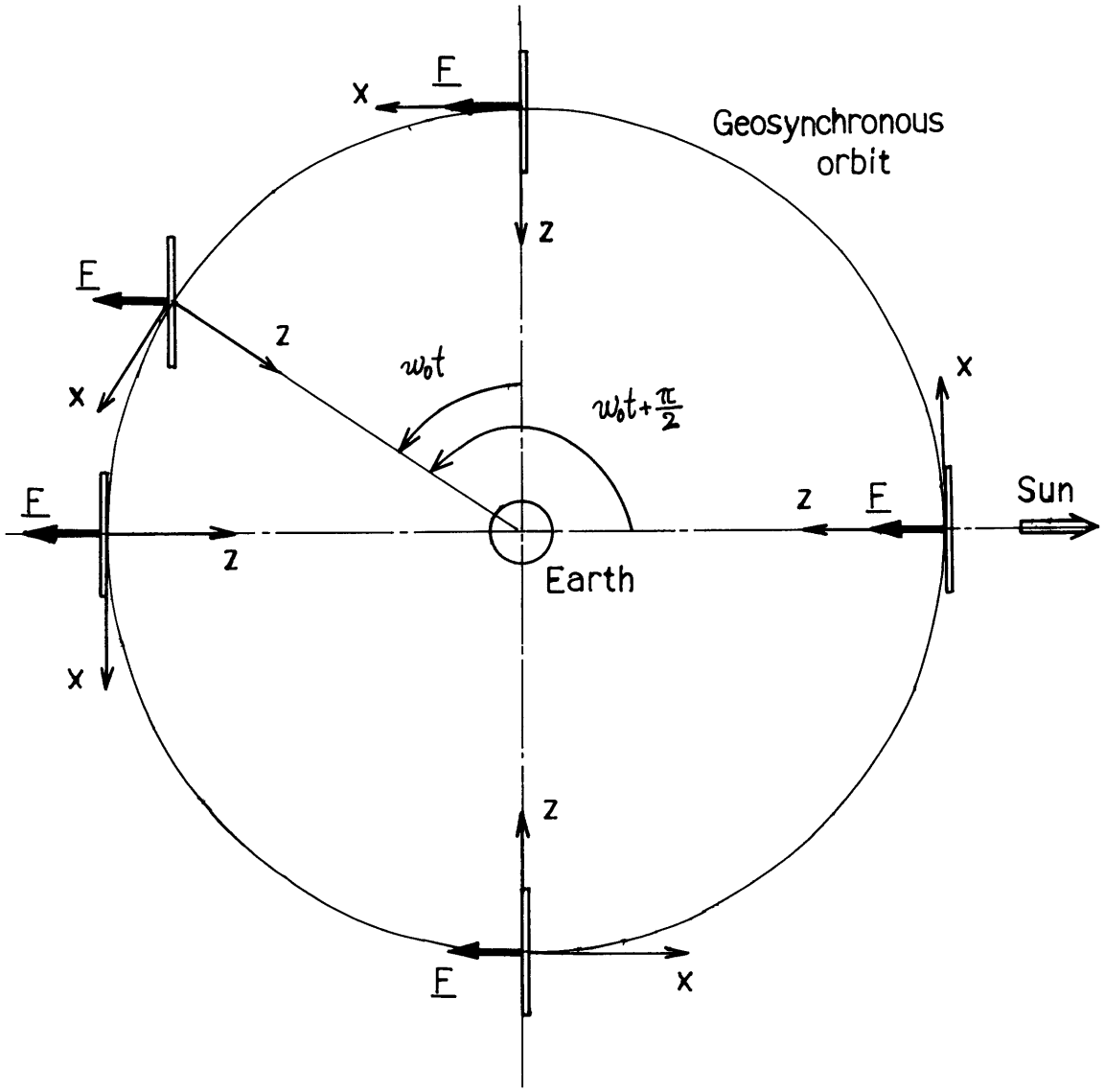

Fig.2.2 Geometrical Relation between the Solar Cell Paddles and the Sun Line

Next, the gravity gradient torque $\underline{G}$ is defined by

$$\underline{G} = \frac{3\mu}{Ro^3} [\underline{1}_{Ro} \times (I \underline{1}_{Ro})] \tag{2.15}$$

where I is the inertia tensor, μ is the gravitational constant, and Ro, $\underline{1}_{Ro}$ are the magnitude and unit vector of the position vector of the spacecraft. In this expression, 'x' represents the vector cross product. For a circular orbit with angular velocity ωo

$$\frac{\mu}{Ro^3} = \omega o^2 \tag{2.16}$$

Since x, y, z axes are principal axes, then x, y, z components of $\underline{G}$ are given in simple form as

$$Gx = 3\omega o^2 (Iz - Iy) a_y a_z \tag{2.17}$$

$$Gy = 3\omega o^2 (Ix - Iz) a_x a_z \tag{2.18}$$

$$Gz = 3\omega o^2 (Iy - Ix) a_x a_y \tag{2.19}$$

where a_x, a_y, a_z are the components of $\underline{1}_{Ro}$.

Now, a set of thrusters is used for attitude corrections. As discussed in Chapter 1, using thrusters will be potentially better than momentum-exchange devices for precise attitude correction because of the fact that the former has no significant moving part. Generally, longer lifetime and higher preciseness of the attitude correction require the thrusters to have higher specific impulse and lower thrust level. For that reason an electrical thruster will be preferable to a chemical thruster. Fig. 2.3 shows a simple allocation of the electrical thrusters.

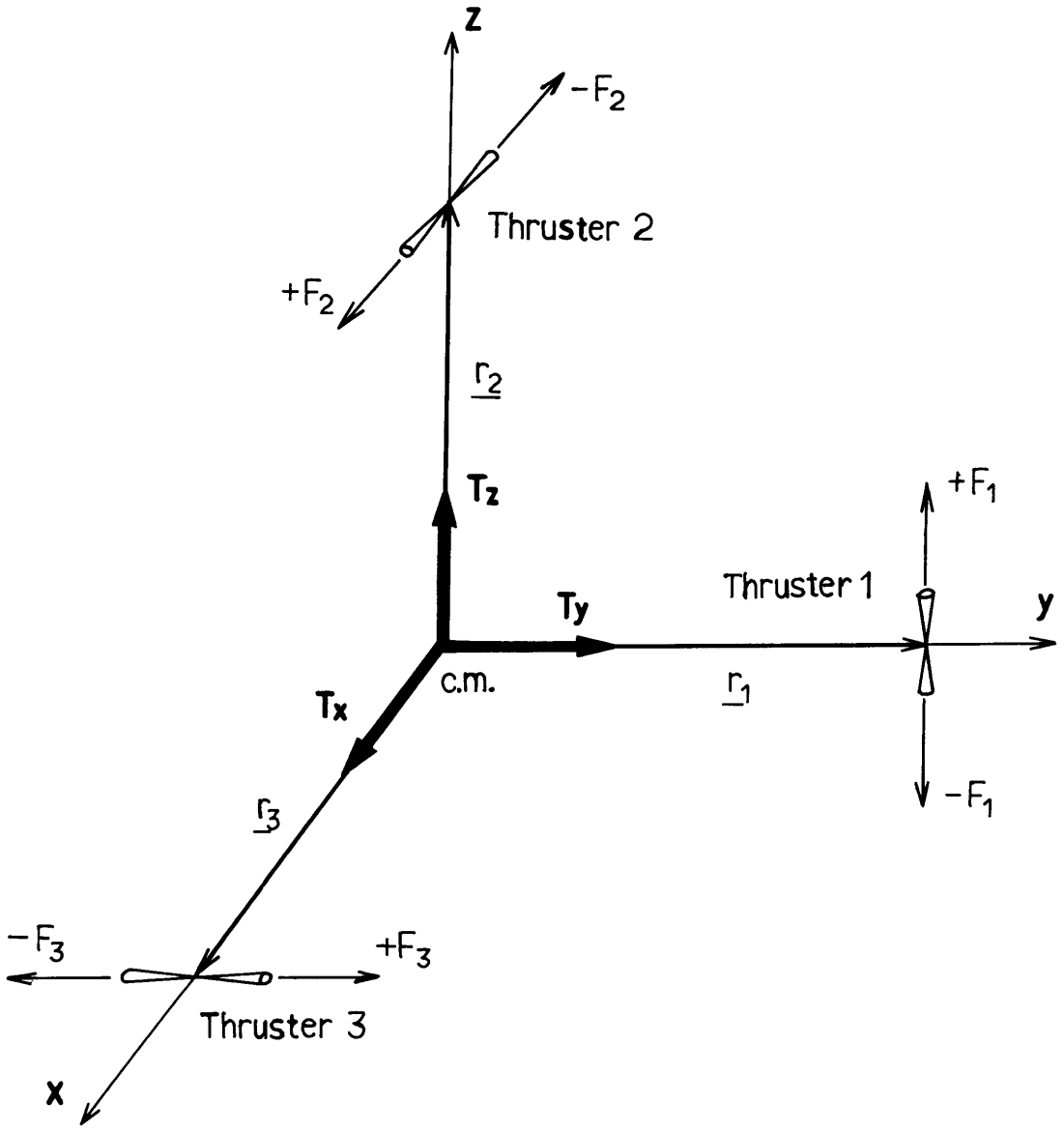

Fig.2.3 Electric Thrusters Location

Because of the complexity of the power supply required to achieve high specific impulse[7] a more complex thruster arrangement, including the possibility of mechanical gimballing, may be desirable. However, for our purpose the allocation defined in Fig. 2.3 is sufficient. Thrusters 1, 2, 3 are used for producing torques about x, y, z axes respectively. The thrusting torque about each axis can be defined by

$$Tx = Txn + \Delta Tx + \xi_1(t) \tag{2.20}$$

$$Ty = Tyn + \Delta Ty + \xi_2(t) \tag{2.21}$$

$$Tz = Tzn + \Delta Tz + \xi_3(t) \tag{2.22}$$

where Txn, Tyn, Tzn are nominal torques produced by each thruster separately which levels are known previously, and ΔTx, ΔTy, ΔTz are torque bias errors caused by level deviations from the nominals, misalignments and couplings from the other thrusters. ξ_1, ξ_2, ξ_3 are random fluctuations in the torque levels which are assumed to be white noises with the intensities Vt_1, Vt_2, Vt_3 respectively.

2.3 Linearization

To linearize the dynamic equations we define a stabilized coordinate frame (designated by 'SF') which is a reference frame on orbit for the body-fixed frame (designated by 'BF') to be stabilized about. The SF has its origin at the mass center of the spacecraft and axes parallel to the position vector and the orbit normal. Fig. 2.4 shows these relations. Fig. 2.4 also shows the definitions of Euler's angles ϕ, θ, Ψ

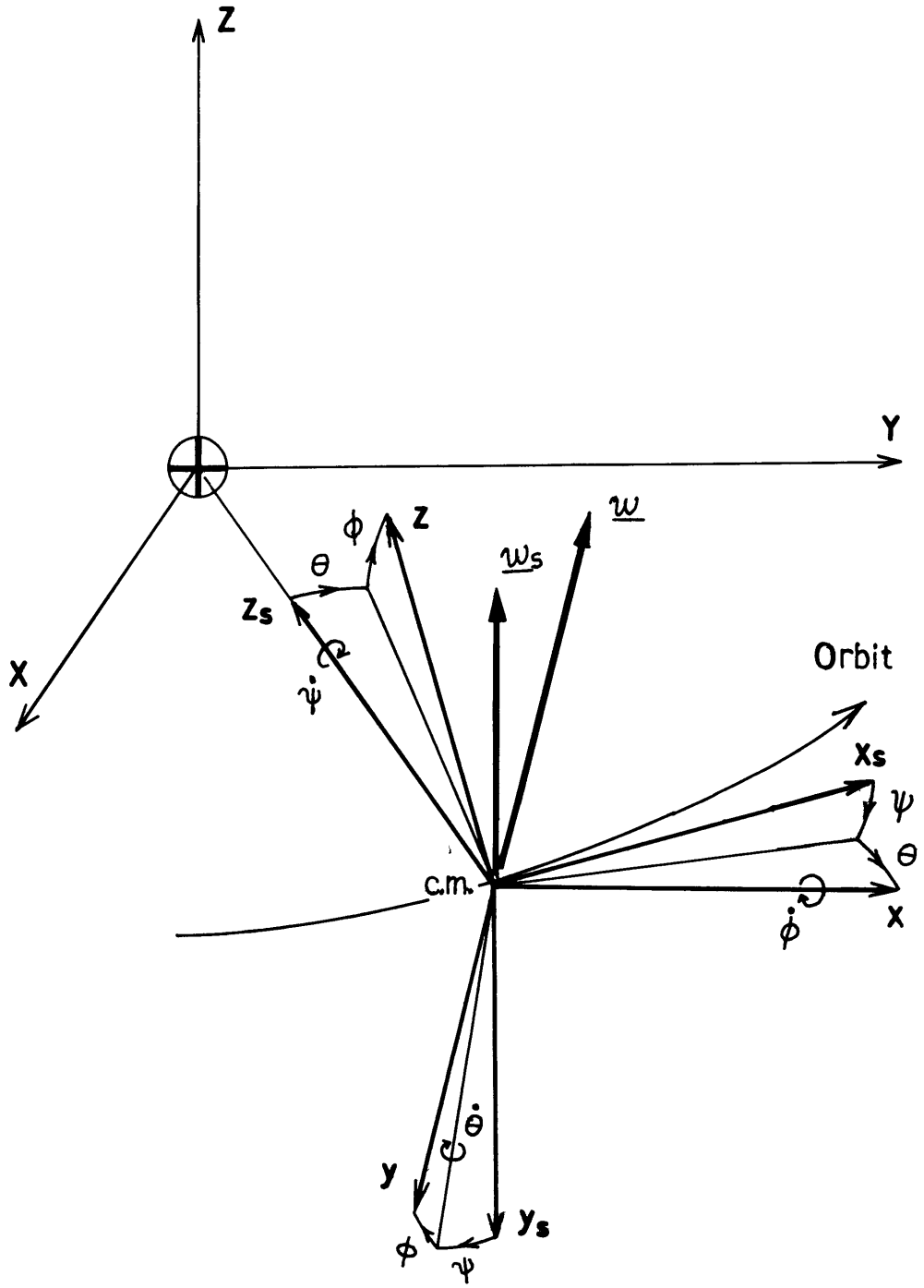

Fig.2.4 Definition of the Coordinate Frames and Euler's Angles

which define a coordinate rotation from SF to BF.

The angular velocity vector of BF with respect to the inertial coordinate frame (designated by IF), $\underline{w}$, is equal to the sum of the angular velocity vector of SF with respect to IF, $\underline{w}_S$, and BF with respect to SF, $\underline{w}_{BS}$. $\underline{w}_{BS}$ can be related to the Euler angle rates $\dot{\phi},\dot{\theta},\dot{\Psi}$ by

$$\underline{w}_{BS}^{(B)} = \begin{bmatrix} 1 & 0 & -\sin\theta \\ 0 & \cos\phi & \cos\theta \sin\phi \\ 0 & -\sin\phi & \cos\theta \cos\phi \end{bmatrix} \begin{bmatrix} \dot{\phi} \\ \dot{\theta} \\ \dot{\psi} \end{bmatrix} \qquad (2.23)$$

Also $\underline{w}_S$ satisfies

$$\underline{w}_S^{(B)} = C_S^B \underline{w}_S^{(S)} \qquad (2.24)$$

where

$$C_S^B = \begin{bmatrix} \cos\psi \cos\theta & \sin\psi \cos\theta & -\sin\theta \\ \cos\psi \sin\theta \sin\phi - \sin\psi \cos\phi & \sin\psi \sin\theta \sin\phi + \cos\psi \cos\phi & \cos\theta \sin\phi \\ \cos\psi \sin\theta \cos\phi + \sin\psi \sin\phi & \sin\psi \sin\theta \cos\phi - \cos\psi \sin\phi & \cos\theta \cos\phi \end{bmatrix} \qquad (2.25)$$

Now, Euler's angles are assumed to be small enough so that $\sin\phi \sim \phi$, $\sin\theta \sim \theta$, $\sin\Psi \sim \Psi$, $\cos\phi \sim \cos\theta \sim \cos\Psi \sim 1$ are satisfied. Then, by using the fact that $\underline{w}_S^{(S)} = (0, -\omega_o, o)^T$ one can easily derive the equation

$$\underline{w}^{(B)} = \begin{bmatrix} wx \\ wy \\ wz \end{bmatrix} = \begin{bmatrix} \dot{\phi} - wo\psi \\ \dot{\theta} - wo \\ \dot{\psi} + wo\phi \end{bmatrix} \qquad (2.26)$$

By substituting Eq. (2.26) and its time derivative into Eq. (2.1), (2.2), (2.3), the following equations result.

$$\left.\begin{aligned} Mx &= Ix\ddot{\phi} - wo(Ix - Iy + Iz)\dot{\psi} + w\delta^2(Iy - Iz)\phi \\ My &= Iy\ddot{\theta} \\ Mz &= Iz\ddot{\psi} + wo(Ix - Iy + Iz)\dot{\phi} + w\delta^2(Iy - Ix)\psi \end{aligned}\right\} \qquad (2.27)$$

where

$$\left.\begin{aligned} Mx &= Gx + Sx + Tx \\ My &= Gy + Sy + Ty \\ Mz &= Gz + Sz + Tz \end{aligned}\right\} \qquad (2.28)$$

Since $\underline{1}_{Ro}^{(S)} = (0, 0, -1)^T$ and $\underline{1}_{Ro}^{(B)} = C_S^B \, \underline{1}_{Ro}^{(S)}$, then Eq. (2.17), (2.18), (2.19) are converted to

$$Gx = -3w\delta^2(Iy - Iz)\phi \qquad (2.29)$$

$$Gy = -3w\delta^2(Ix - Iz)\theta \qquad (2.30)$$

$$Gz = -3w\delta^2(Iy - Ix)(\theta\phi) \simeq 0 \qquad (2.31)$$

Therefore, Eq. (2.27) becomes

$$Sx + Tx = Ix\ddot{\phi} - wo(Ix - Iy + Iz)\dot{\psi} + 4w\delta^2(Iy - Iz)\phi \qquad (2.32)$$

$$Sy + Ty = Iy\ddot{\theta} + 3w\delta^2(Ix - Iz)\theta \qquad (2.33)$$

$$Sz + Tz = Iz\ddot{\psi} + wo(Ix - Iy + Iz)\dot{\phi} + w\delta^2(Iy - Ix)\psi \qquad (2.34)$$

Define the state vector to be

$$\underline{x} \equiv \begin{bmatrix} \phi \\ \theta \\ \psi \\ \dot{\phi} \\ \dot{\theta} \\ \dot{\psi} \end{bmatrix} \tag{2.35}$$

Then Eq. (2.32), (2.33), (2.34) divided by Ix, Iy, Iz respectively yield

$$\dot{\underline{x}} = A\underline{x} + B(\underline{S} + \underline{T}) \tag{2.36}$$

where

$$A = \begin{bmatrix} 0 & 0 & 0 & 1 & 0 & 0 \\ 0 & 0 & 0 & 0 & 1 & 0 \\ 0 & 0 & 0 & 0 & 0 & 1 \\ -4\omega_o^2 a & 0 & 0 & 0 & 0 & \omega_o(1-a) \\ 0 & -3\omega_o^2 b & 0 & 0 & 0 & 0 \\ 0 & 0 & -\omega_o^2 c & \omega_o(c-1) & 0 & 0 \end{bmatrix} \tag{2.37}$$

$$a = \frac{Iy - Iz}{Ix} \tag{2.38}$$

$$b = \frac{Ix - Iz}{Iy} \tag{2.39}$$

$$c = \frac{Iy - Ix}{Iz} \tag{2.40}$$

$$B = \begin{bmatrix} 0 & 0 & 0 \\ 0 & 0 & 0 \\ 0 & 0 & 0 \\ 1/Ix & 0 & 0 \\ 0 & 1/Iy & 0 \\ 0 & 0 & 1/Iz \end{bmatrix} \qquad (2.41)$$

2.4 Observation Equations

There exist some possible combinations of measurements such as (ϕ, θ, Ψ), $(\dot{\phi}, \dot{\theta}, \dot{\Psi})$, etc., for use in state estimation. But for precise attitude estimation during the station keeping phase, an angle rate measurement is likely to be less sensitive. That leads us to use angle measurements.

Two edge-tracking type horizon sensors are assumed to measure the roll and pitch angles respectively. Since there are weak couplings between roll and yaw, the yaw angle may be left free if no strict specification exists on it. However, large yaw angle rate may disturb the mission in such a way that it distorts an image taken by a scanning spectrometer. Therefore a star-tracker which detects Polaris is assumed to measure the yaw angle. Actually if we were to use nonlinear filtering technique, no star tracker might be needed. But it is not essential for our problem. Fig. 2.5 shows the measurement configuration using optical sensors.

Usually an optical sensor output contains not only measurement noise but measurement bias due to optical axis misalignment.

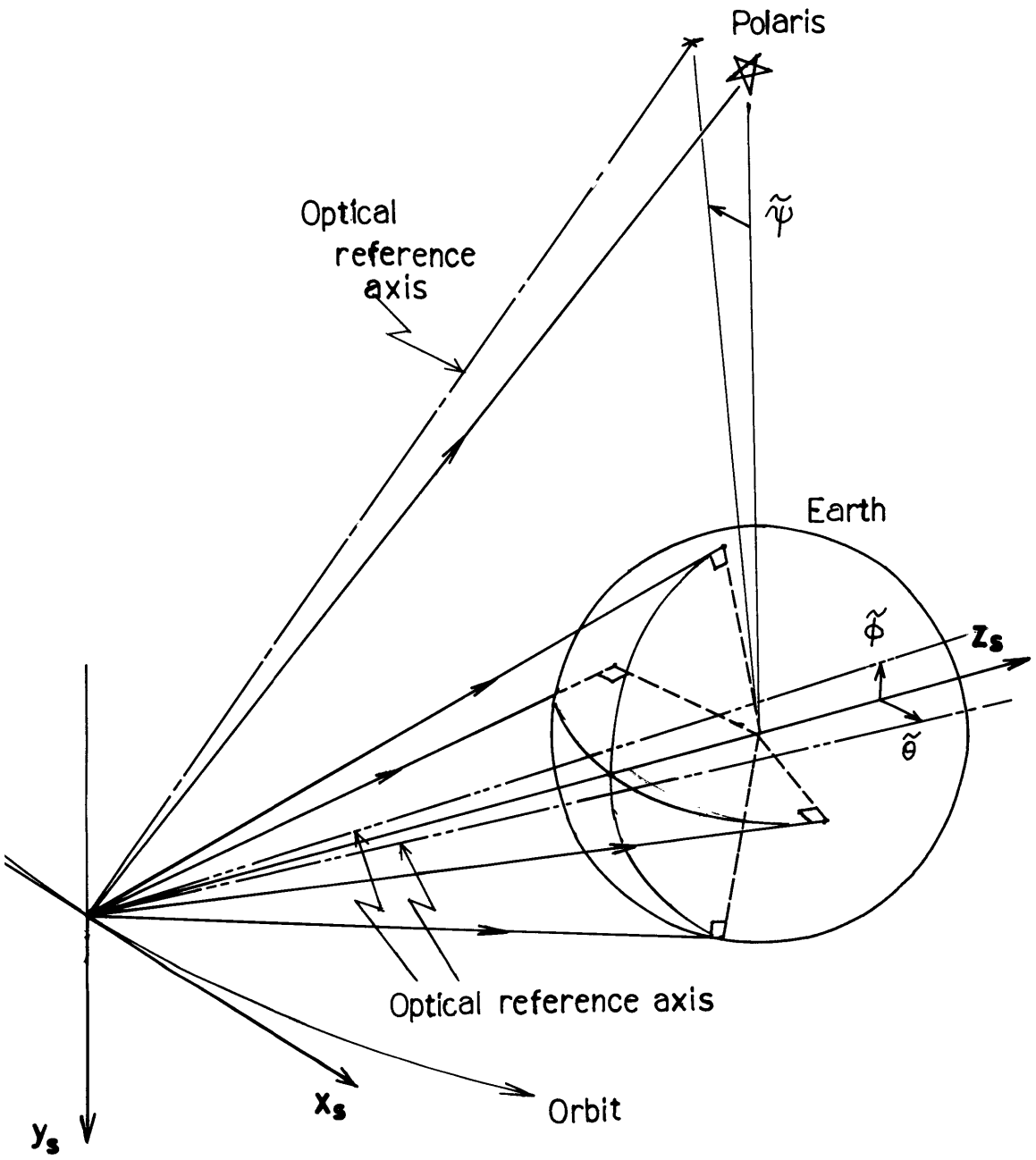

Fig.2.5 Geometrical relations of the Observations

Here we take account of only the dominant bias errors such as roll angle bias, $\delta\phi$, for the roll measurement, pitch angle bias, $\delta\theta$, for the pitch measurement and yaw angle bias, $\delta\Psi$, for the yaw measurement.

Therefore the observation equations are of the form

$$\begin{bmatrix} \tilde{\phi} \\ \tilde{\theta} \\ \tilde{\psi} \end{bmatrix} = D\underline{x} + \begin{bmatrix} \delta\phi \\ \delta\theta \\ \delta\psi \end{bmatrix} + \begin{bmatrix} \eta x \\ \eta y \\ \eta z \end{bmatrix} \qquad (2.42)$$

where

$$D = \begin{bmatrix} 1 & 0 & 0 & 0 & 0 & 0 \\ 0 & 1 & 0 & 0 & 0 & 0 \\ 0 & 0 & 1 & 0 & 0 & 0 \end{bmatrix} \qquad (2.43)$$

and ηx, ηy, ηz are measurement noises which, we assume, are white noise with the intensity of Vmx, Vmy, Vmz respectively.

2.5 Discrete-Time State Equations and Output Equations

The solar pressure torque equations given by Eq. (2.10), (2.11), (2.12) and the thruster torque equations given by Eq. (2.21), (2.22), (2.23) are rewritten in vector form as

$$\underline{S} = \begin{bmatrix} Sx \\ Sy \\ Sz \end{bmatrix} = \begin{bmatrix} -\sin\omega ot & 0 \\ 0 & \cos\omega ot + \kappa\sin\omega ot \\ -\cos\omega ot & 0 \end{bmatrix} \begin{bmatrix} bsx \\ bsy \end{bmatrix} \qquad (2.44)$$

$$\underline{T} = \begin{bmatrix} Tx \\ Ty \\ Tz \end{bmatrix} = \underline{U}n + \begin{bmatrix} \Delta Tx \\ \Delta Ty \\ \Delta Tz \end{bmatrix} + \begin{bmatrix} \xi_1(t) \\ \xi_2(t) \\ \xi_3(t) \end{bmatrix} \qquad (2.45)$$

where

$$\kappa = \frac{xt}{zt} \qquad (2.46)$$

$$\underline{U}n = \begin{bmatrix} Txn \\ Tyn \\ Tzn \end{bmatrix} \qquad (2.47)$$

Since our principal objective is to estimate Sx, Sy, Sz, we have to treat them as augmented states. However, the augmented state equations contain unknown coefficients. Then we had better estimate bsx, bsy indirectly by treating them as constant bias states. Note κ can be determined operationaly by

$$\frac{xt}{zt} = \frac{\hat{b}sy(\text{at } \omega ot = \frac{\pi}{2})}{\hat{b}sy(\text{at } \omega ot = 0)} = \frac{xtFo}{ztFo} \qquad (2.48)$$

Now we define a bias vector $\underline{b}$ by

$$\underline{b} \equiv \begin{bmatrix} bsx \\ bsy \\ \Delta Tx \\ \Delta Ty \\ \Delta Tz \\ \delta\phi \\ \delta\theta \\ \delta\psi \end{bmatrix} \tag{2.49}$$

Then from Eq. (2.37), (2.43), (2.45), (2.46) the continuous-time state equations and output equations are represented by

$$\dot{\underline{x}}(t) = A\underline{x}(t) + B\underline{u}n + C(t)\underline{b} + B\underline{w}t(t) \tag{2.50}$$

$$\underline{y}(t) = D\underline{x}(t) + E\underline{b} + \underline{w}m(t) \tag{2.51}$$

where

$$C(t) = \left[\begin{array}{ccc:ccc:c} 0 & 0 & & 0 & 0 & 0 & \\ 0 & 0 & & 0 & 0 & 0 & \\ 0 & 0 & & 0 & 0 & 0 & \\ -\frac{1}{Ix}\sin\omega ot & 0 & & \frac{1}{Ix} & 0 & 0 & O_{6\times 3} \\ 0 & \frac{1}{Iy}(\cos\omega ot+\kappa\sin\omega ot) & & 0 & \frac{1}{Iy} & 0 & \\ -\frac{1}{Iz}\cos\omega ot & 0 & & 0 & 0 & \frac{1}{Iz} & \end{array}\right] \tag{2.52}$$

$$E = [O_{3\times 5} \vdots I_{3\times 3}] \tag{2.53}$$

Also, $\underline{wt}(t)$, $\underline{wm}(t)$ are the thrusting torque noise vector $(\xi_1(t), \xi_2(t), \xi_3(t))^T$ and measurement noise vector $(\eta_1(t),\eta_2(t),\eta_3(t))^T$ respectively, and both are white noises with the intensity matrices of

$$Vt = \begin{bmatrix} Vt_1 & 0 & 0 \\ 0 & Vt_2 & 0 \\ 0 & 0 & Vt_3 \end{bmatrix} \tag{2.54}$$

$$Vm = \begin{bmatrix} Vm_1 & 0 & 0 \\ 0 & Vm_2 & 0 \\ 0 & 0 & Vm_3 \end{bmatrix} \tag{2.55}$$

If the moments of inertia Ix, Iy, Iz are constants, the matrix A becomes constant. Then the corresponding transition matrix, $\Phi(t,\tau)$, is given by

$$\Phi(t, \tau) = e^{A(t-\tau)} = \Phi(t-\tau) \tag{2.56}$$

Actually the variations in the moments of inertia associated with the rotation of the solar cell paddles with respect to the main body and the fuel consumption, are considered to be small. For example, the variation due to the paddle rotation for a typical spacecraft of interest is less than 1% of the total moment. Therefore it is reasonable to assume that Ix, Iy, Iz are constants.

Now we can use Eq. (2.56) for discretizing the state equation (2.50). If we assume a constant sampling period T, the discrete-time state difference equations can be derived from the solution equation of Eq. (2.50) in the form

$$\underline{x}(t_{i+1}) = e^{AT}\underline{x}(t_i) + (\int_{t_i}^{t_{i+1}} e^{A(t_{i+1}-\tau)}d\tau)\, B\underline{u}n + (\int_{t_i}^{t_{i+1}} e^{A(t_{i+1}-\tau)}$$

$$C(\tau)d\tau)\underline{b} + \int_{t_i}^{t_{i+1}} e^{A(t_{i+1}-\tau)} B\underline{wt}(\tau)d\tau \qquad (2.57)$$

For a small T, $C(\tau)$ in Eq. (2.57) can be replaced by $C(t_i)$ since $C(\tau) \simeq C(t_i)$ for $t_i < \tau < t_{i+1} = t_i + T$.

The fourth term in the right hand side of Eq. (2.57) is a zero-mean, mutually uncorrelated stochastic sequence[8] with variance matrix

$$Vt(i) = \int_{t_i}^{t_{i+1}} e^{A(t_{i+1}-\tau)} BVtB^T e^{A^T(t_{i+1}-\tau)} d\tau \qquad (2.58)$$

The sequence is designated by $\underline{wt}(i)$, that is,

$$\underline{wt}(i) \equiv \int_{t_i}^{t_{i+1}} e^{A(t_{i+1}-\tau)} B\underline{wt}(\tau)d\tau \qquad (2.59)$$

Actually Vt(i) is constant here. The second and third terms in the right hand side of Eq. (2.57) have the same integral factor which one can easily prove to be

$$\int_{t_i}^{t_{i+1}} e^{A(t_{i+1}-\tau)} d\tau = A^{-1}[e^{AT}-I] \qquad \text{for all ti} \geq \text{to} \qquad (2.60)$$

Therefore the discrete-time state difference equation is of the form

$$\underline{x}(i+1) = Ad\underline{x}(i) + Bd\underline{u}(i) + Cd(i)\underline{b} + \underline{wt}(i) \qquad (2.61)$$

where

$$Ad = e^{AT} \qquad (2.62)$$

$$Bd = A^{-1}[e^{AT} - I]B \qquad (2.63)$$

$$Cd = A^{-1}[e^{AT} - I]C(ti) \tag{2.64}$$

$$\underline{u}(i) = \underline{\mathbf{u}}n \tag{2.65}$$

The detailed forms of Ad, Bd, Cd are summarized in Appendix A.

If we assume a synchronous sampling, the discrete-time output equation is described by

$$\underline{y}(i) = D\underline{x}(i) + E\underline{b} + \underline{w}m(i) \tag{2.65}$$

where $\underline{w}m(i)$ is a zero-mean, mutually uncorrelated stochastic sequence with constant variance matrix Vm.

CHAPTER 3

'SEPARATE-BIAS' KALMAN FILTER

In the previous chapter we derived the discrete-time state difference equation and the output equation. We have to estimate the bias vector $\underline{b}$ defined by Eq. (2.49) in addition to the state vector $\underline{x}$. However, since the order of $\underline{b}$ exceeds that of $\underline{x}$, a regular state augmentation method will not be the most efficient way to estimate bsx, bsy, bsz accurately.

An augmented states Kalman filter would have to treat a state vector of order 14 instead of 6. This would introduce numerical inaccuracies due to the handling of large vectors and matrices. In addition to that the computational speed may be severely compromised. B. Friedland devised a so-called 'Separate-Bias' Kalman filter in which the bias estimation is essentially decoupled from the estimation of the prime states. Since this filter deals with reduced order vectors and matrices, the associated numerical inaccuracies and compromise in computational speed can be avoided. Therefore we use this method instead of a regular augmentation method.

The 'Separate-Bias' Kalman filter is computationally separated into two parts — 'bias-free state estimation' and 'bias estimation'. The bias-free state estimation part is a standard Kalman filter having no bias terms and estimates the prime states without corrections by any biases. The bias estimation part inputs bias-free residuals calculated in the previous part and estimates each bias. The Kalman gain for the bias estimation is calculated from the bias covariance matrix, the variance matrix of the measurement and the bias-free Kalman gain. The bias corrected state estimate is then given by $\underline{\hat{x}}(i) = \underline{\tilde{x}}(i) + Vx(i)\underline{\hat{b}}(i)$, where $\underline{\tilde{x}}(i)$ is the bias-free state estimate and $\underline{\hat{b}}(i)$ is the bias estimate.

Since the two parts of the 'Separate-Bias' Kalman filter are computationally separated, it has an operational advantage in that two computers could be used in which one computes the bias-free state estimate and the corresponding bias-free residuals while the other computes the bias estimate. Consequently the over-all computational speed would be considerably improve.

Now the discrete-time state equation and output equation are summarized as

$$\underline{x}(i+1) = Ad\underline{x}(i) + Bd\underline{u}(i) + Cd(i)\underline{b} + \underline{w}_t(i) \tag{3.1}$$

$$\underline{b}(i+1) = \underline{b}(i) \tag{3.2}$$

$$\underline{y}(i) = D\underline{x}(i) + E\underline{b} + \underline{w}_m(i) \tag{3.3}$$

$$E[\underline{w}_t(i) \cdot \underline{w}_t^T(i)] = V_t \tag{3.4}$$

$$E[\underline{w}_m(i) \cdot \underline{w}_m^T(i)] = V_m \tag{3.5}$$

The "Separate-Bias" Kalman Filter is described by:

Bias-Free Residual;

$$\tilde{\underline{r}}(i) = \underline{y}(i) - DAd\tilde{\underline{x}}(i-1) - DBd\underline{u}(i-1) \tag{3.6}$$

Bias-Free Gain;

$$\tilde{K}x(i) = \tilde{P}\bar{x}\ (i)D^T[D\tilde{P}\bar{x}\ (i)D^T + V_m]^{-1} \tag{3.7}$$

Bias-Free Estimate;

$$\tilde{\underline{x}}(i) = Ad\tilde{\underline{x}}(i-1) + Bd\underline{u}(i-1) + \tilde{K}x(i)\tilde{\underline{r}}(i) \tag{3.8}$$

$$\tilde{\underline{x}}(0) = E[\underline{x}(0)] \tag{3.9}$$

Bias-Free Covariance Matrix;

$$\tilde{\bar{P}}_x(i+1) = Ad\tilde{T}_x(i)Ad^T + Vt \tag{3.10}$$

$$\tilde{T}_x(i) = [I-\tilde{K}_x(i)D]\ \tilde{\bar{P}}_x(i) \tag{3.11}$$

Bias Gain;

$$Kb(i) = M(i+1)\ [V\tilde{\bar{x}}(i)D^T + E^T]\ V_m^{-1} \tag{3.12}$$

Bias Estimate;

$$\underline{\hat{b}}(i) = [I - Kb(i)S(i)]\underline{\hat{b}}(i-1) + Kb(i)\underline{\tilde{r}}(i) \tag{3.13}$$

$$\underline{\hat{b}}_0 = E[\underline{b}_0] \tag{3.14}$$

Bias-Corrected State Estimate;

$$\underline{\hat{x}}(i) = \underline{\tilde{x}}(i) + Vx(i)\underline{\hat{b}}(i) \tag{3.15}$$

Bias Covariance Matrix;

$$M(i+1) = M(i)-M(i)S^T(i)[D\tilde{\bar{P}}_x(i)D^T+V_m+S(i)M(i)S^T(i)]^{-1}S(i)M(i) \tag{3.79}$$

where

$$Ux(i+1) = AdVx(i) + Cd(i) \tag{3.80}$$

$$S(i) = DUx(i) + E \tag{3.81}$$

$$Vx(i) = Ux(i) - \tilde{K}x(i)S(i) \tag{3.82}$$

Fig. 3.1 shows the data flow of the real time "Separate Bias' Kalman filter.

Fig.3.1 Flow Chart of the 'Separate Bias' Kalman Filter Computation (Real Time)

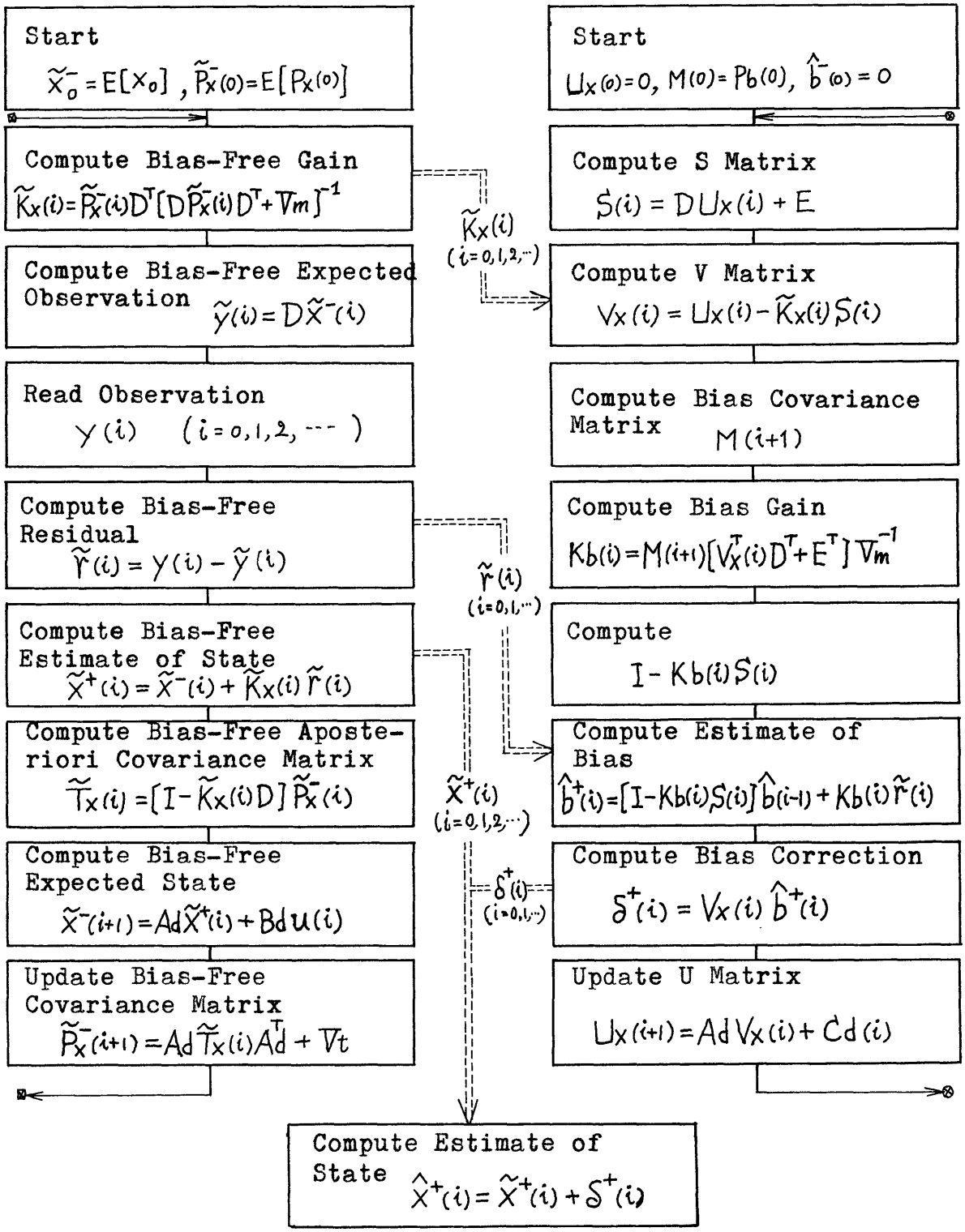

CHAPTER 4

REAL TIME OPTIMAL CONTROL LAW

4.1 Control Decision Table

The real time optimal control law discussed in this chapter achieves the maximum soft limit cycle period by determining each thrust on/off time from observation of whether a state trajectory predicted from the current state and bias estimates reaches the specified angle limit or not. The state trajectories to be predicted are of two types: a thrust-free trajectory for the thrust-off timing determination and a thrusting trajectory for the thrust-on timing determination. Fig. 4.1 shows those relations.

To construct the control law one has to take account of the fact that the solar pressure torque components may vary and change their signs during a thrust-free phase. Therefore, we need a simple control decision table to make the decision of which thrust on/off timing calculation should be made. That table is given in Table 4.1. The estimated solar pressure torque components are used to see which direction each trajectory is facing, whereas the current state estimates are used to see in which quadrant of the phase plane the state is located.

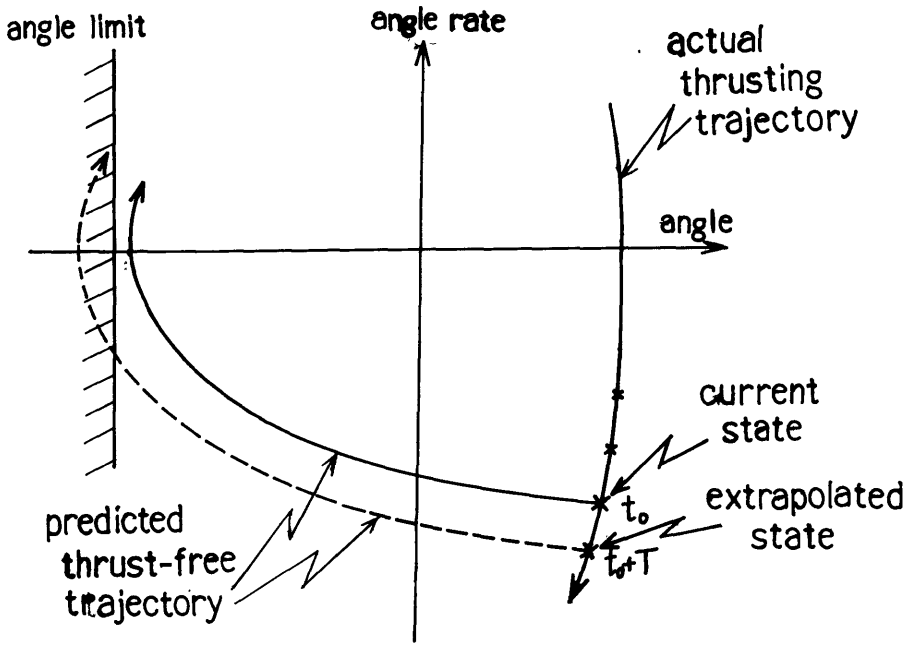

Thrust-Off Determination

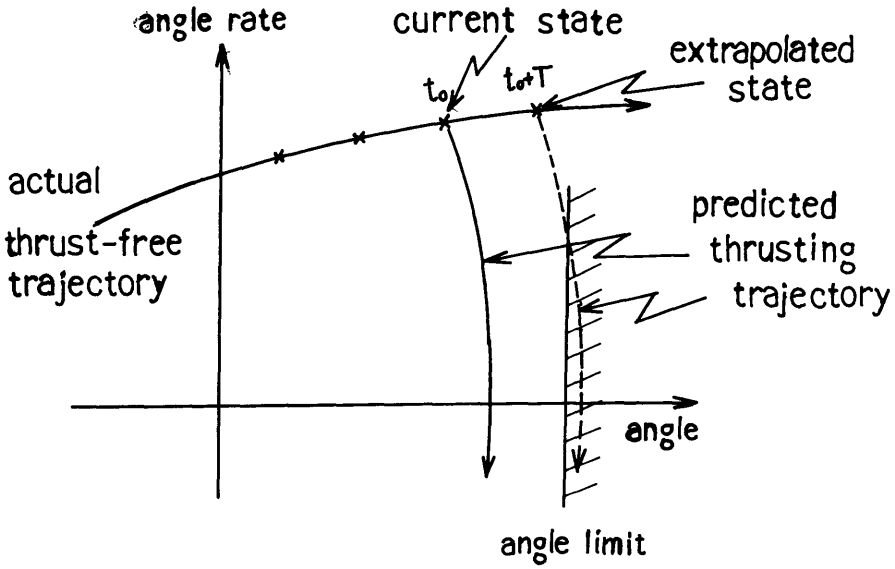

Thrust-On Determination

Fig.4.1 Relation between Actual and Predicted State Trajectory

Table 4.1 Control Decision Table

Current Status				Thrust Control Requirement
Angle	Angle Rate	Solar Pressure Torque Component	Thrusting	
+	+	+ or 0.0	Off	(-) Thrusting on
−	−	− or 0.0	Off	(+) Thrusting on
——	——	——	(+) Thrusting on	Thrusting off
——	——	——	(-) Thrusting on	Thrusting off

4.2 Trajectory Prediction

The trajectory predictions are done by approximated linear dynamic equations.

From Eq. (2.32), (2.33), (2.34) the linearized dynamic equations are given in the form

$$\ddot{\phi}(t) + w_0(a-1)\dot{\Psi}(t) + 4w_0 a\phi(t) = Mx(t) \tag{4.1}$$

$$\ddot{\theta}(t) + 3w_0^2 b\theta(t) = My(t) \tag{4.2}$$

$$\ddot{\Psi}(t) + w_0(1-c)\dot{\phi}(t) + w_0^2 c\Psi(t) = Mz(t) \tag{4.3}$$

Since $a \sim c \sim -1$, $b \sim 0$, $w_0 \sim 10^{-4}$, $(Sx/Ix)/(4w_0^2 a\phi)\ 10^{+2}$, and $(Sy/Iy)/(3w_0^2 b\theta) \sim (Sz/Iz)/(w_0^2 c\Psi) \sim 10^{+4}$, then additional approximation is possible; that is, w_0^2 terms can be neglected so as to yield

$$\ddot{\phi}(t) + w_0(a-1)\dot{\Psi}(t) = Mx(t) \tag{4.4}$$

$$\ddot{\theta}(t) = My(t) \tag{4.5}$$

$$\ddot{\Psi}(t) + w_0(1-c)\dot{\phi}(t) = Mz(t) \tag{4.6}$$

By integrating Eq.(4.4), (4.5), (4.6), one can easily derive

$$\dot{\phi}(t) = \dot{\phi}(t_0) + 2\alpha\dot{\Psi}(t_0)(t-t_0) + 2\alpha\int_{t_0}^{t}(t-\xi)Mz(\xi)d\xi + \int_{t_0}^{t}Mx(\xi)d\xi \tag{4.7}$$

$$\dot{\theta}(t) = \dot{\theta}(t_0) + \int_{t_0}^{t} My(\xi)d\xi \tag{4.8}$$

$$\dot{\Psi}(t) = \dot{\Psi}(t_0) + 2\beta\dot{\phi}(t_0)(t-t_0) + 2\beta\int_{t_0}^{t}(t-\xi)Mx(\xi)d\xi + \int_{t_0}^{t}Mz(\xi)d\xi \tag{4.9}$$

$$\phi(t) = \phi(t_0) + \dot{\phi}(t_0)(t-t_0) + \alpha\dot{\Psi}(t_0)(t-t_0)^2 + \alpha\int_{t_0}^{t}(t-\xi)^2Mz(\xi)d\xi + \int_{t_0}^{t}(t-\xi)Mx(\xi)d\xi \tag{4.10}$$

$$\theta(t) = \theta(t_0) + \dot{\theta}(t_0)(t-t_0) + \int_{t_0}^{t}(t-\xi)My(\xi)d\xi \tag{4.11}$$

$$\Psi(t) = \Psi(t_0) + \dot{\Psi}(t_0)(t-t_0) + \beta\dot{\phi}(t_0)(t-t_0)^2 + \beta\int_{t_0}^{t}(t-\xi)^2Mx(\xi)d\xi + \int_{t_0}^{t}(t-\xi)Mz(\xi)d\xi \tag{4.12}$$

Where

$$\alpha = -\frac{1}{2}w_0(\alpha-1) \tag{4.13}$$

$$\beta = -\frac{1}{2}w_0(1-c) \tag{4.14}$$

An advantageous point of these approximated equations is that they are decoupled so that each angle and angle rate can be predicted from the current state estimates and forcing terms only.

For simplicity we make another approximation. In a thrust-free trajectory prediction of a certain axis, only the solar pressure torque is included in the forcing terms even though there is a possibility of cross-coupling torques due to thrusting in other axes. Also in a thrusting trajectory prediction, only the thrusting torque terms are included.

Consequently, by putting

$$Mx(t) = -\frac{\hat{b}sx}{Ix}\sin w_0 t \tag{4.15}$$

$$My(t) = \frac{\hat{b}sy}{Iy}(\cos w_0 t + \hat{\kappa}\sin w_0 t) \tag{4.16}$$

$$Mz(t) = -\frac{\hat{b}sx}{Iz}\cos w_0 t \tag{4.17}$$

Where $\hat{b}_{sx}$, $\hat{b}_{sy}$, $\hat{\kappa}$ are current estimated biases, the equations for the thrust-free trajectory prediction are given as follows.

$$\phi(t) = \phi(t_0) + \dot{\phi}(t_0)(t-t_0) + \alpha\dot{\Psi}(t_0)(t-t_0)^2 - \alpha\beta_3 f_2(t,t_0) + \beta_1 g_1(t,t_0) \tag{4.18}$$

$$\theta(t) = \theta(t_0) + \dot{\theta}(t_0)(t-t_0) + \beta_2 g_2(t-t_0) - \beta_4 g_1(t,t_0) \tag{4.19}$$

$$\Psi(t) = \Psi(t_0) + \dot{\Psi}(t_0)(t-t_0) + \beta\dot{\phi}(t_0)(t-t_0)^2 + \beta\beta_1 f_1(t,t_0) - \beta_3 g_2(t,t_0) \tag{4.20}$$

$$\dot{\phi}(t) = \dot{\phi}(t_0) + 2\alpha\dot{\Psi}(t_0)(t-t_0) - 2\alpha\beta_3 g_2(t,t_0) + \beta_1 h_1(t,t_0) \tag{4.21}$$

$$\dot{\theta}(t) = \dot{\theta}(t_0) + \beta_2 h_2(t,t_2) - \beta_4 h_1(t,t_0) \tag{4.22}$$

$$\dot{\Psi}(t) = \dot{\Psi}(t_0) + 2\beta\dot{\phi}(t_0)(t-t_0) + 2\beta\beta_1 g_1(t,t_0) - \beta_3 h_2(t,t_0) \tag{4.23}$$

$$f_1(t,t_0) = -\frac{2}{w_0^3}[\cos w_0 t - \{1 - \frac{w_0^2}{2}(t-t_0)^2\} \cos w_0 t_0 + w_0(t-t_0) \sin w_0 t_0] \quad (4.24)$$

$$f_2(t,t_0) = \frac{2}{w_0^3}[-\sin w_0 t + \{1 - \frac{w_0^2}{2}(t-t_0)^2\} \sin w_0 t_0 + w_0(t-t_0) \cos w_0 t_0] \quad (4.25)$$

$$g_1(t,t_0) = -\frac{1}{w_0^2}[w_0(t-t_0) \cos w_0 t_0 - \sin w_0 t + \sin w_0 t_0] \quad (4.26)$$

$$g_2(t,t_0) = -\frac{1}{w_0^2}[w_0(t-t_0) \sin w_0 t_0 + \cos w_0 t - \cos w_0 t_0] \quad (4.27)$$

$$h_1(t,t_0) = \frac{1}{w_0}[\cos w_0 t - \cos w_0 t_0] \quad (4.28)$$

$$h_2(t,t_0) = \frac{1}{w_0}[\sin w_0 t - \sin w_0 t_0] \quad (4.29)$$

where $\beta_1 = \hat{b}sx/Ix$, $\beta_2 = \hat{b}sy/Iy$, $\beta_3 = \hat{b}sx/Iz$

$\beta_4 = \beta_2 \cdot \hat{\kappa}$

In the same manner, by putting

$$Mx(t) = (Tx_n + \Delta\hat{T}x) / Ix \tag{4.30}$$

$$My(t) = (Ty_n + \Delta\hat{T}y) / Iy \tag{4.31}$$

$$Mz(t) = (Tz_n + \Delta\hat{T}z) / Iz \tag{4.32}$$

where $\Delta\hat{T}x$, $\Delta\hat{T}y$, $\Delta\hat{T}z$ are the estimated biases, the equations for the thrusting trajectory prediction are given as follows.

$$\phi(t) = \phi(t_0) + \dot{\phi}(t_0)(t-t_0) + \{\alpha\dot{\Psi}(t_0) + \frac{1}{2}(\frac{Tx}{Ix}\} (t-t_0)^2 + \frac{\alpha}{3}(\frac{Tz}{Iz})(t-t_0)^3 \tag{4.33}$$

$$\theta(t) = \theta(t_0) + \dot{\theta}(t_0)(t-t_0) + \frac{1}{2}(\frac{Ty}{Iy})(t-t_0)^2 \tag{4.34}$$

$$\Psi(t) = \Psi(t_0) + \dot{\Psi}(t_0)(t-t_0) + \{\beta\dot{\phi}(t_0) + \frac{1}{2}(\frac{Tz}{Iz})\} (t-t_0)^2 + \frac{\beta}{3}(\frac{Tx}{Ix})(t-t_0)^3 \tag{4.35}$$

$$\dot{\phi}(t) = \dot{\phi}(t_0) + \{2\alpha\dot{\Psi}(t_0) + (\frac{Tx}{Ix})\} (t-t_0) + \alpha(\frac{Tz}{Iz})(t-t_0) \tag{4.36}$$

$$\dot{\theta}(t) = \dot{\theta}(t_0) + (\frac{Ty}{Iy})(t-t_0) \tag{4.37}$$

$$\dot{\Psi}(t) = \dot{\Psi}(t_0) + \{2\beta\dot{\phi}(t_0) + (\frac{Tz}{Iz})\} (t-t_0) + \beta(\frac{Tx}{Ix})(t-t_0)^2 \tag{4.38}$$

where

$$Tx = Txn + \Delta\hat{T}x$$

$$Ty = Tyn + \Delta\hat{T}y \qquad (4.39)$$

$$Tz = Tzn + \Delta\hat{T}z$$

4.3 Thrust On/Off Timing Determination

Once a thrust on/off decision for any axis is required by the control decision table, one predicts the trajectory using the equations defined in the previous section, which would result from taking the control action at each sampling instant. Comparison of the maximum angle excursion on this predicted trajectory with the specified error angle limit determines whether or not the control action should be taken at that time.

The author proposes the following algorithm. (Note only the logic for the roll angle is described here, but the other angles have the same algorithm.)

∘ Thrust-Off Timing Determination

(a) Extrapolate the current state to the point one sampling period later, $\phi(t_0 + T)$, $\dot{\phi}(t_0 + T)$, by Eq. (4.33), (4.36), where t_0, T are current time and sampling period.

(b) Set $t_0 = t_0 + T$ and $\hat{\dot{\phi}}(t_0) = \dot{\phi}(t_0 + T)$.

(c) Assume the termination of thrusting. Calculate the time t_1 at which the angle rate will become zero, $\dot{\phi}(t_1) = 0$, by

$$t_1 \simeq t_0 - \left(\frac{Ix}{Sx}\right) \hat{\dot{\phi}}\ (t_0) \qquad (4.39)$$

$$Sx = - \hat{b}_{sx} \sin w_0 t_0 \qquad (4.40)$$

If $|t_1| > R_\phi$, execute the thrust-off command, where $R\phi$ is a positive large number.

(d) Compute $\phi(t_1)$ and $\dot{\phi}(t_1)$ by Eq. (4.18), (4.21).

(e) If $|\dot{\phi}(t_1)| > \varepsilon_\phi$, set $t_0 = t_1$ and iterate from (c) to (e).

If $|\dot{\phi}(t_1)| \leq \varepsilon_\phi$, go to (f).

where ε_ϕ is a positive small number.

(f) Compare the predicted angle, $\phi(t_1)$, with the angle limit $\phi_L(>0)$ in following way. Compute

$$\Delta\phi = \begin{cases} \phi_L + \phi(t_1) & \text{if} \quad Sx > 0 \\ \phi_L - \phi(t_1) & \text{if} \quad Sx < 0 \end{cases} \tag{4.41}$$

(g) If $\Delta\phi \leq 0$, execute the thrust-off command.

If $\Delta\phi > 0$, no action should be taken.

◦ Thrust-On Timing Determination

(a) The same as in (a) of Thrust-Off Timing Determination, except using Eq. (4.18), (4.21) instead of Eq. (4.33), (4.36).

(b) The same as in (b) of Thrust-Off Timing Determination.

(c) Assume the firing of the thruster. Calculate the time t_1 at which the angle rate will become zero, $\dot{\phi}(t_1) = 0$, by

$$t_1 \simeq t_0 - \left(\frac{Ix}{Tx}\right) \hat{\dot{\phi}}(t_0) \qquad (4.42)$$

$$Tx = Tx_n + (\text{the latest } \hat{\Delta Tx}) \qquad (4.43)$$

(d) Compute $\phi(t_1)$ and $\dot{\phi}(t_1)$ by Eq. (4.33), (4.36)

(e) The same as in (e) of Thrust-Off Timing Determination.

(f) The same as in (f) of Thrust-Off Timing Determination, except using Tx instead of Sx.

(g) If $\Delta\phi \leq 0$, execute the thrust-on command.
If $\Delta\phi > 0$, no action should be taken.

In (c) of Thrust-Off Timing Determination R_ϕ is determined based on the accuracy of the trajectory prediction equations. Here $|t_1| > R_\phi$ occurs when $Sx \simeq 0$.

CHAPTER 5

CALCULATIONS AND RESULTS

5.1 Spacecraft Attitude Simulator

In this chapter the simulation results which reveal the feasibility and performance characteristics of the attitude control scheme discussed in previous chapters are presented.

Before presenting the results, we discuss briefly a spacecraft simulator which generates the attitude data. From Euler's moment equations given by Eq. (2.1), (2.2), (2.3), and Eq. (2.10) $\sim$ (2.12), (2.20) $\sim$ (2.24), one can derive the following first order nonlinear differential equations.

$$\dot{w}_x = awywz - 3w_0^2 a \cos^2\theta \sin\phi \cos\phi - \left(\frac{bsx}{Ix}\right) \sin w_0 t + \left(\frac{1}{Ix}\right) \xi_1(t) + \frac{1}{Ix}(Txn + \Delta Tx) \quad (5.1)$$

$$\dot{w}y = -bw_x w_z - 3w_0^2 b \sin\theta \cos\theta \cos\phi + \left(\frac{bsy}{Iy}\right)\left(\cos w_0 t + \frac{xt}{zt} \sin w_0 t\right) + \left(\frac{1}{Iy}\right) \xi_2(t) + \frac{1}{Iy}(Tyn + \Delta Ty) \quad (5.2)$$

$$\dot{w}z = -cw_x w_y - 3w_0^2 c \sin\theta \cos\theta \sin\phi - \left(\frac{bsz}{Iz}\right) \cos w_0 t + \left(\frac{1}{Iz}\right) \xi_3(t) + \frac{1}{Iz}(Tzn + \Delta Tz) \quad (5.3)$$

$$\dot{\phi} = w_x + w_y \sin\phi \tan\theta + w_z \cos\phi \tan\theta + w_0(\frac{\sin\Psi}{\cos\theta}) \tag{5.4}$$

$$\dot{\theta} = w_y \cos\phi - w_z \sin\phi + w_0 \cos\Psi \tag{5.5}$$

$$\dot{\Psi} = w_y(\frac{\sin\phi}{\cos\theta}) + w_y(\frac{\cos\phi}{\cos\theta}) + w_0 \sin\Psi \tan\theta \tag{5.6}$$

Since Eq. (5.1), (5.2), (5.3) include white noise terms, those equations should be separated into two parts when they are intergrated.

$$\dot{w}_x = \dot{w}_{xd} + \delta\dot{w}_x \tag{5.7}$$

$$\dot{w}_y = \dot{w}_{yd} + \delta\dot{w}_y \tag{5.8}$$

$$\dot{w}_z = \dot{w}_{zd} + \delta\dot{w}_z \tag{5.9}$$

where $\dot{w}_{xd}$, $\dot{w}_{yd}$, $\dot{w}_{zd}$ are equal to the deterministic parts of Eq. (5.1), (5.2), (5.3) respectively, and $\delta\dot{w}_x + \xi_1/I_x$, $\delta\dot{w}_y = \xi_2/I_y$, $\delta\dot{w}_z = \xi_3/I_z$

Using the fact that the integral of a zero-mean, white noise stochastic process is a random walk,[9] we can write the solutions of Eq. (t.7), (5.8), (5.9) in discrete-time form approximately as

$$w_x(t_{k+1}) = w_{xd}\ (t_{k+1}) + \zeta_1(t_k) \tag{5.10}$$

$$w_y(t_{k+1}) = w_{yd}\ (t_{k+1}) + \zeta_2(t_k) \tag{5.11}$$

$$w_z(t_{k+1}) = w_{zd}\ (t_{k+1}) + \zeta_3(t_k) \tag{5.12}$$

where ζ_1, ζ_2, ζ_3, are zero-mean, mutually uncorrelated stochastic sequence with variances of

$$V_{\zeta 1} = (\frac{1}{I_x})^2\ V_{t1} \cdot H \tag{5.13}$$

$$V_{\zeta 2} = (\frac{1}{Iy})^2\ V_{t2} \cdot H \tag{5.14}$$

$$V_{\zeta 3} = (\frac{1}{Iz})^2\ V_{t3} \cdot H \tag{5.15}$$

H is the integration step size.

The deterministic solutions $w_{xd}(t_{k+1})$, $w_{yd}(t_{k+1})$, $w_{zd}(t_{k+1})$ are calculated numerically using the Runge-Kutta fourth order method.

The observation data are simulated simply by

$$\tilde{\phi}(t_i) = \phi(t_i) + \eta_x(t_i) + \delta\phi \tag{5.16}$$

$$\tilde{\theta}(t_i) = \theta(t_i) + \eta y(t_i) + \delta\theta \tag{5.17}$$

$$\tilde{\Psi}(t_i) = \Psi(t_i) + \eta z(t_i) + \delta\Psi \tag{5.18}$$

where $\phi(t_i)$, $\theta(t_i)$, $\Psi(t_i)$ are solutions of the Runge-Kutta integration, $\eta(t_i)$, $\eta(t_i)$, $\eta(t_i)$ are zero-mean, mutually uncorrelated, measurement noises with the variances of V_{mx}, V_{my}, V_{mz}, and $\delta\phi$, $\delta\theta$, $\delta\Psi$ are constant biases of the sensors.

5.2 Configuration and Parameters of the Simulation Program

Fig. 5.1 shows the overall configuration of the simulation program. The parameters used in the program are summarized in Table 5.1.

Each time the operational mode is changed from the thrust-free mode in which no thrusts are used, to the thrusting mode in which at least one of the thrusters is on, or in reverse, the sampling period is changed from 25 seconds to 1 second, or from 1 second to 25 seconds, respectively. At the same time the thrusting torque bias estimates and variances are initialized as follows. At the time of the mode change from thrusting to thrust-free, the initial estimates $\hat{\Delta Tx}$, $\hat{\Delta Ty}$, $\hat{\Delta Tz}$, the variances and covariances, and corresponding elements in the matrix Ux are all set to zeroes. At the time of the mode change from thrust-free to thrusting, the initial estimates, the covariances and corresponding elements in Ux are left zeroes, but the variances are set as

$$M_{33} = \{ \ 0.1 \cdot Txn \ \}^2 + \{ \ 0.03 \ (Tyn + Tzn) \ \}^2 \qquad (5.19)$$

$$M_{44} = \{ \ 0.2 \cdot Tyn \ \}^2 + \{ \ 0.03 \ (Txn + Tzn) \ \}^2 \qquad (5.20)$$

$$M_{55} = \{ \ 0.1 \cdot Tzn \ \}^2 + \{ \ 0.03 \ (txn + Tyn) \ \}^2 \qquad (5.21)$$

For the other biases no initialization is performed at each mode change.

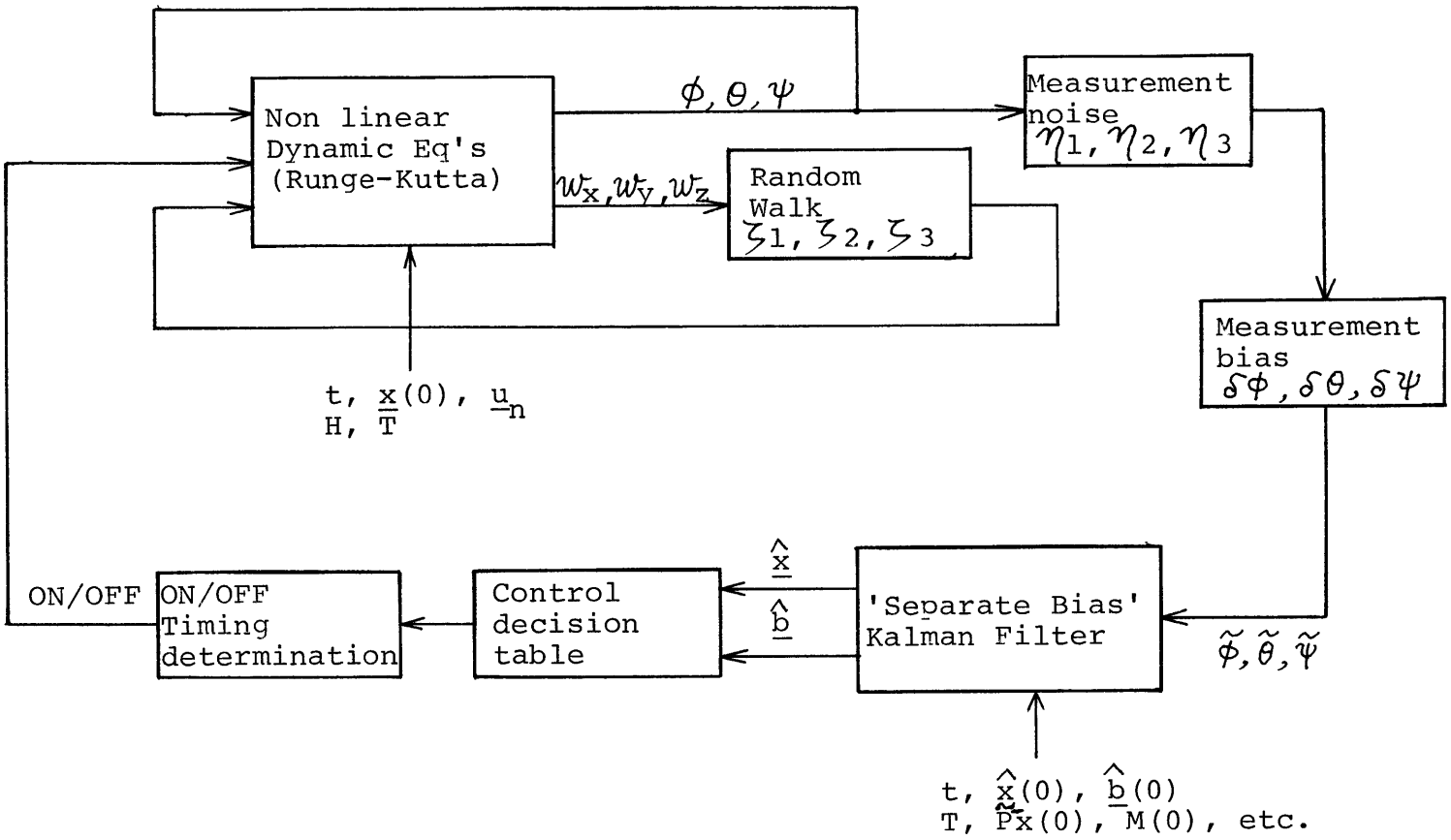

Figure 5.1 Overall Configuration of the Simulation

Table 5.1 Parameters Set of the Simulation

ITEMS	UNITS	VALUES	COMMENTS
Ix	$N \cdot m \cdot s^2$	2000.0	
Iy	"	400.0	
Iz	"	2000.0	
F_o	N	0.0002	Solar pressure magnitude
xt	m	0.1	Solar pressure center position vector components in BF.
yt	"	0.1	
zt	"	0.1	
Txn	N·m	0.000445	Nominal thrust torque level
Tyn	"	0.00011	
Tzn	"	0.000445	
Vt1	$(N \cdot m)^2/Hz$	(5% of the nominal)^2/Hz	Thruster noise intensity
Vt2	"	"	
Vt3	"	"	
ΔTx	N·m	10% of the nominal	Thrust bias
ΔTy	"	"	
ΔTz	"	"	
$\delta\phi$	rad	0.000052	
$\delta\Theta$	rad	0.000052	
$\delta\psi$	rad	0.000052	
Vmx	rad^2	0.3045×10^{-9}	
Vmy	"	"	
Vmz	"	"	

Table 5.1 Parameters Set of the Simulation (Continued)

ITEMS	UNITS	VALUES	COMMENTS
T	sec	25 1	For thrust-free phase For thrusting phase
H	sec	25 1	} Integration step sizes
t_0	sec	23000	$w_0 t_0$ = 95.8 degree
ϕ_{limit}	rad	0.0008727	= 0.05 degree
θ_{limit}	"	0.0008727	= 0.05 degree
ψ_{limit}	"	0.005235	= 0.3 degree
w_0	1/sec	0.00007272205	= 2π /24 [1/HR]

5.3 Simulation Results

The simulation is performed while the spacecraft is located in a region on orbit for which $\frac{\pi}{2} < \text{wot} < \frac{3\pi}{2}$ and continued for 4000 sec. At this point the solar pressure torgue about the roll axis is large but that about the yaw axis is very small. Fig. 5.2, 5.4, 5.6 are the results of the true state trajectories represented in the phase plane. And Fig. 5.3, 5.5 are the histories of the estimation errors for roll and pitch axes respectively.

The estimated biases are shown in Fig. 5.7, 5.8, 5.9.

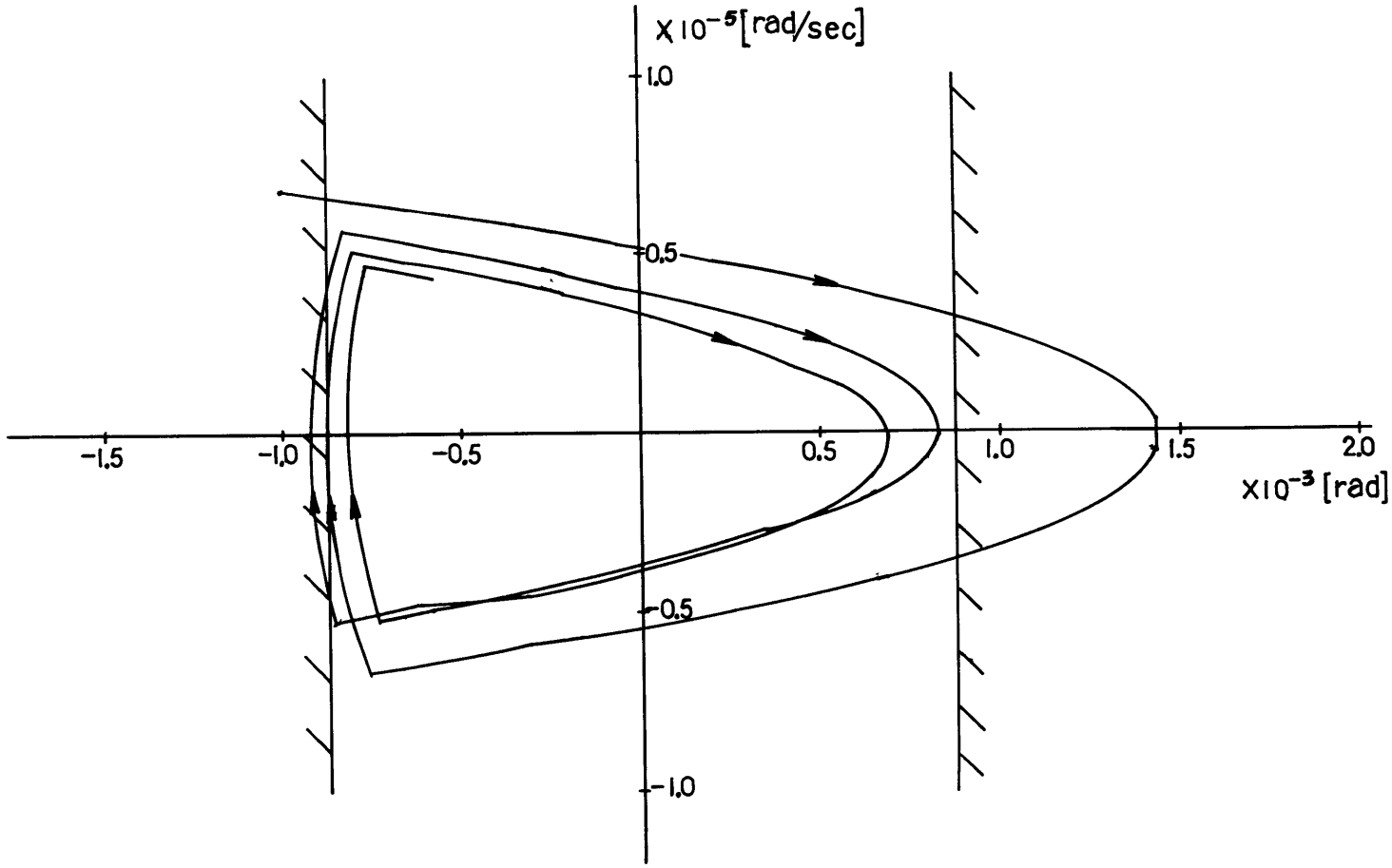

Figure 5.2 Roll Axis True State Trajectory

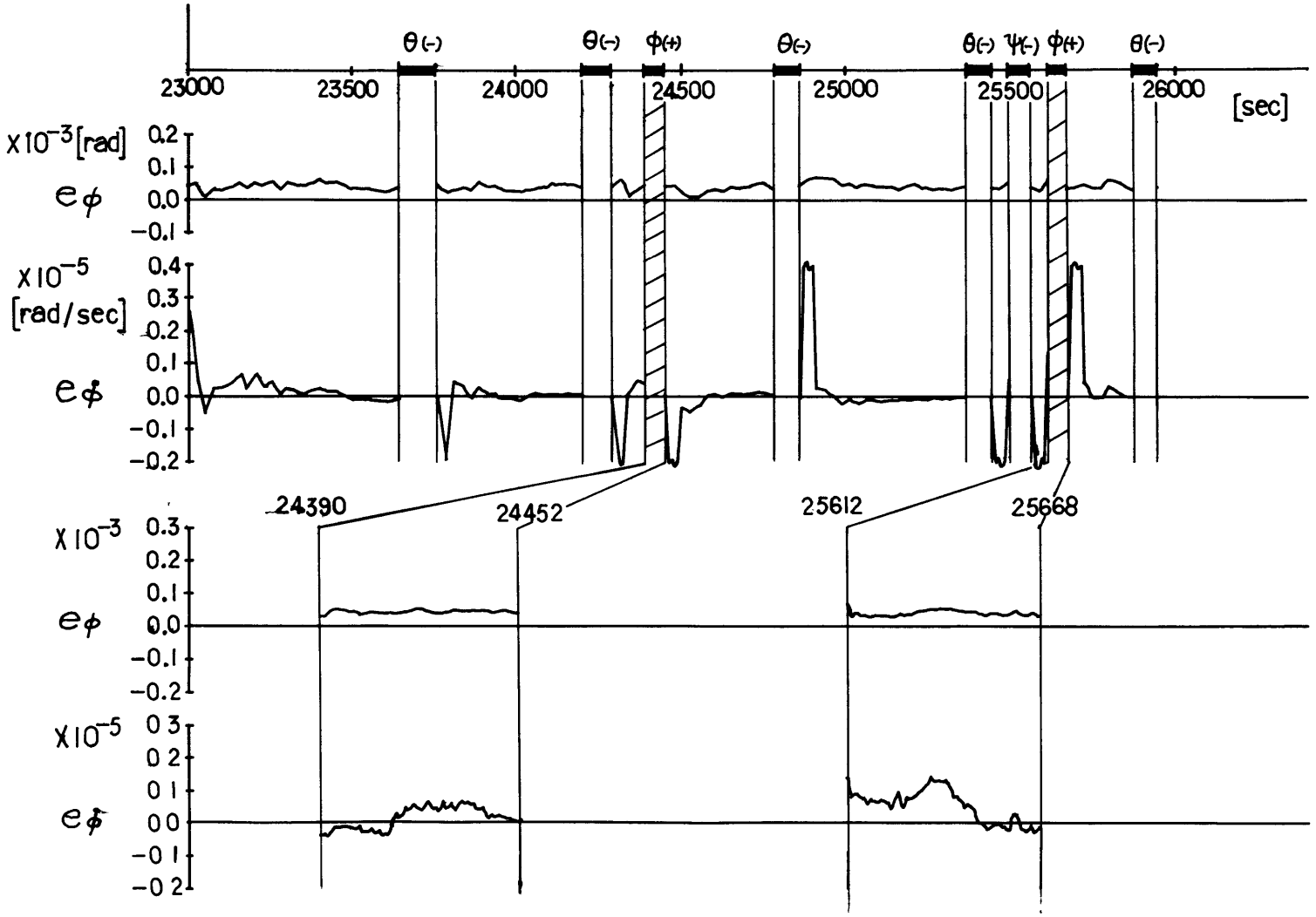

Figure 5.3 Roll Axis Estimation Errors

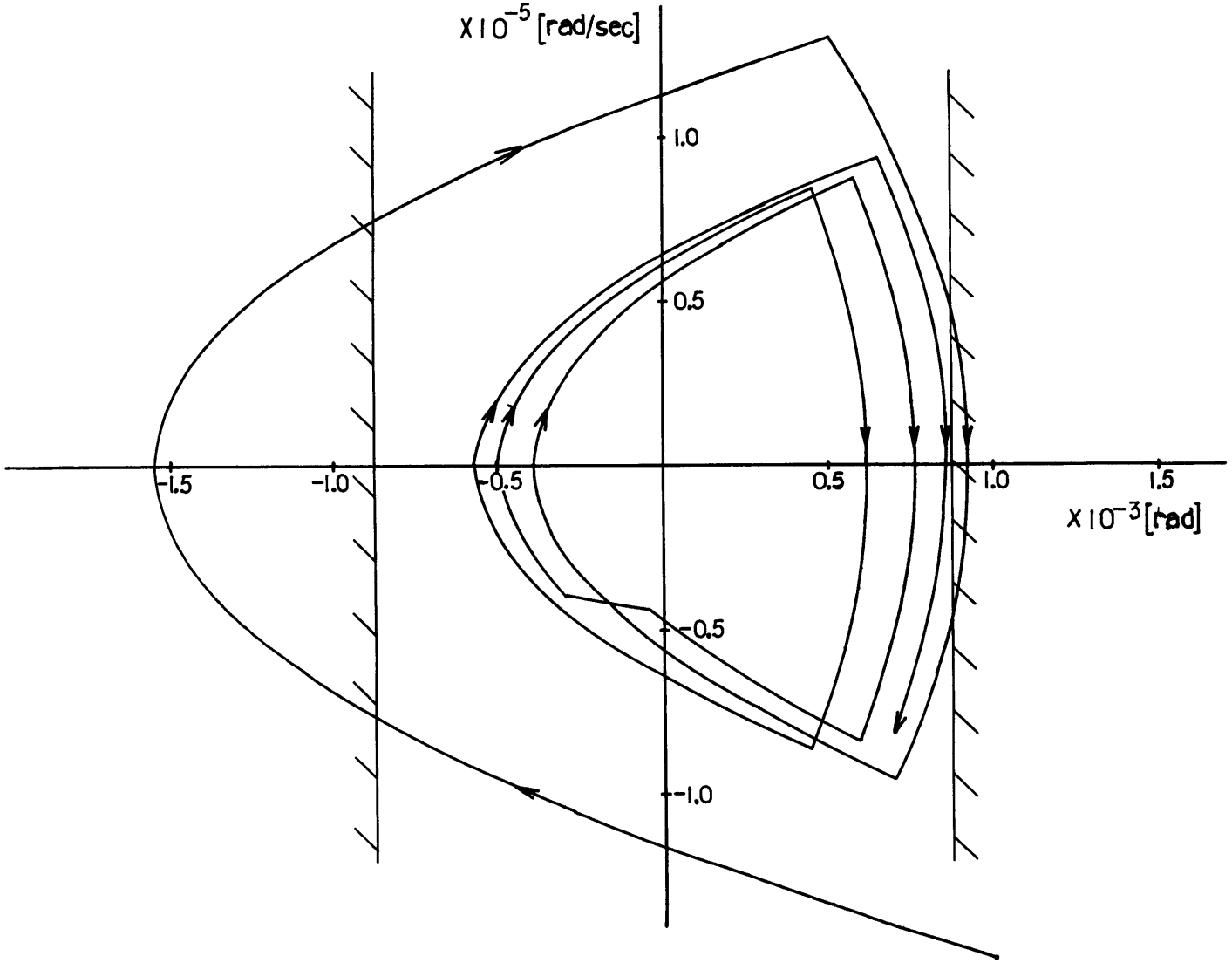

Figure 5.4 Pitch Axis True State Trajactory

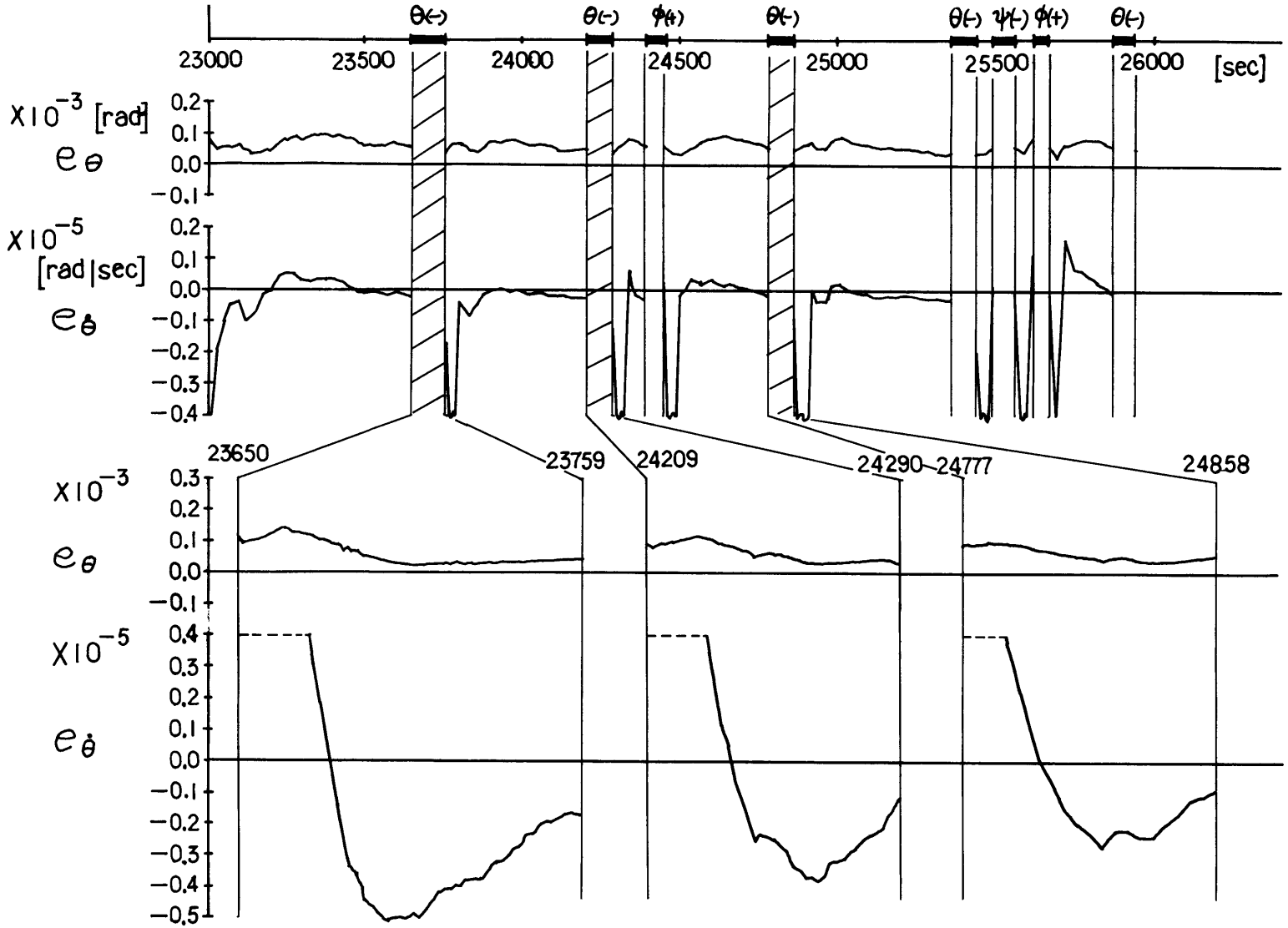

Figure 5.5 Pitch Axis Estimation Errors

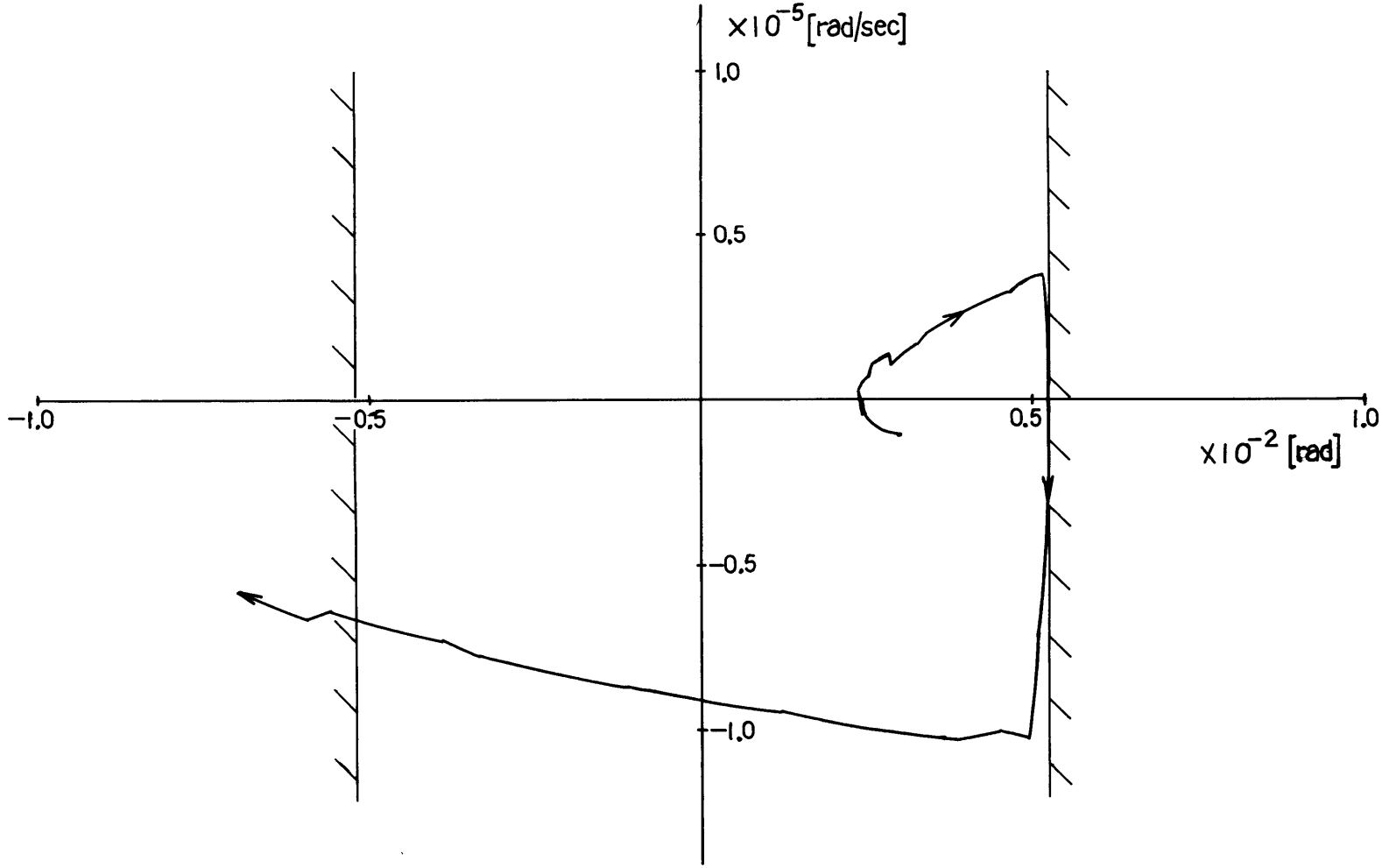

Figure 5.6 Yaw Axis True State Trajectory

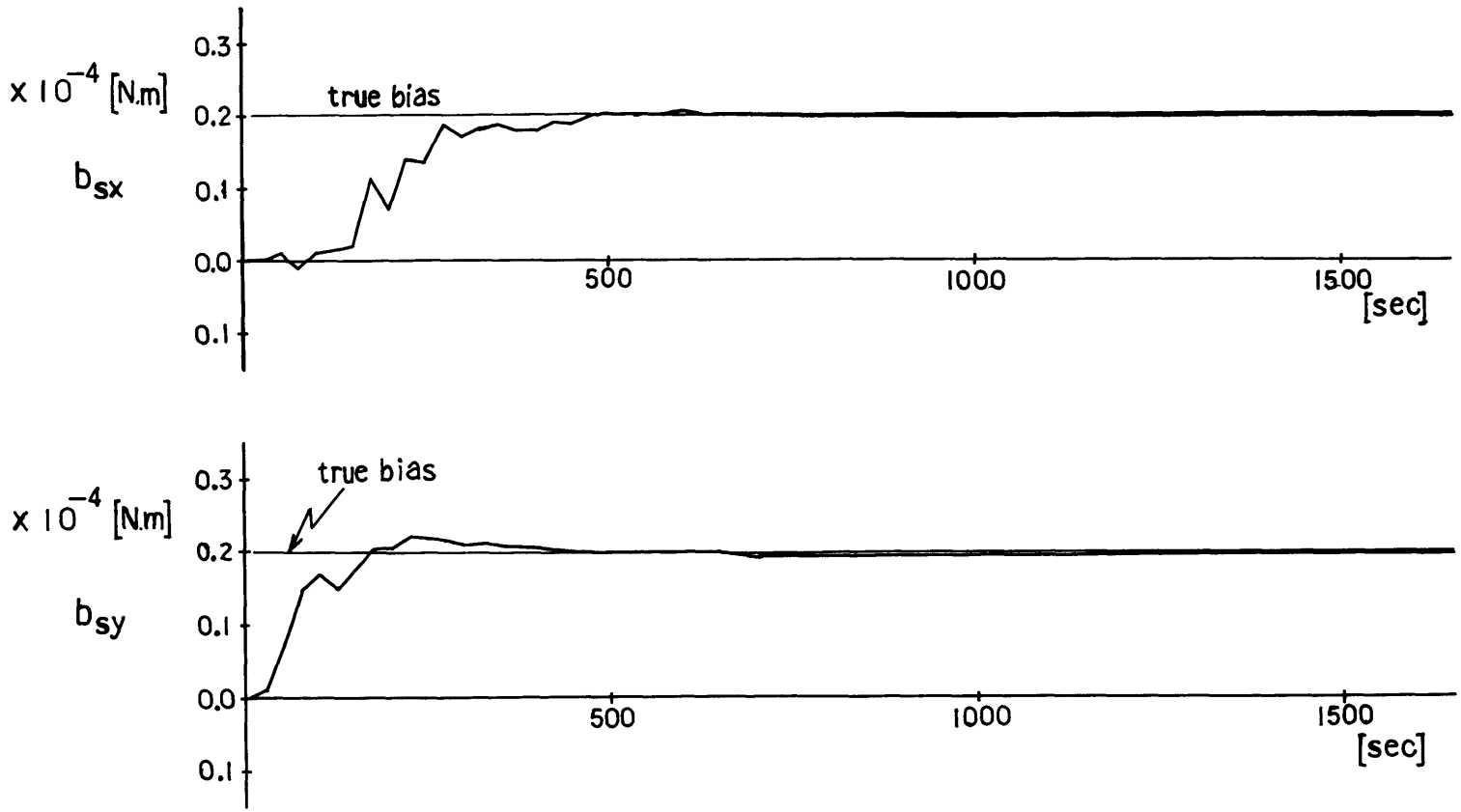

Figure 5.7 Solar Pressure Torque Bias Estimates

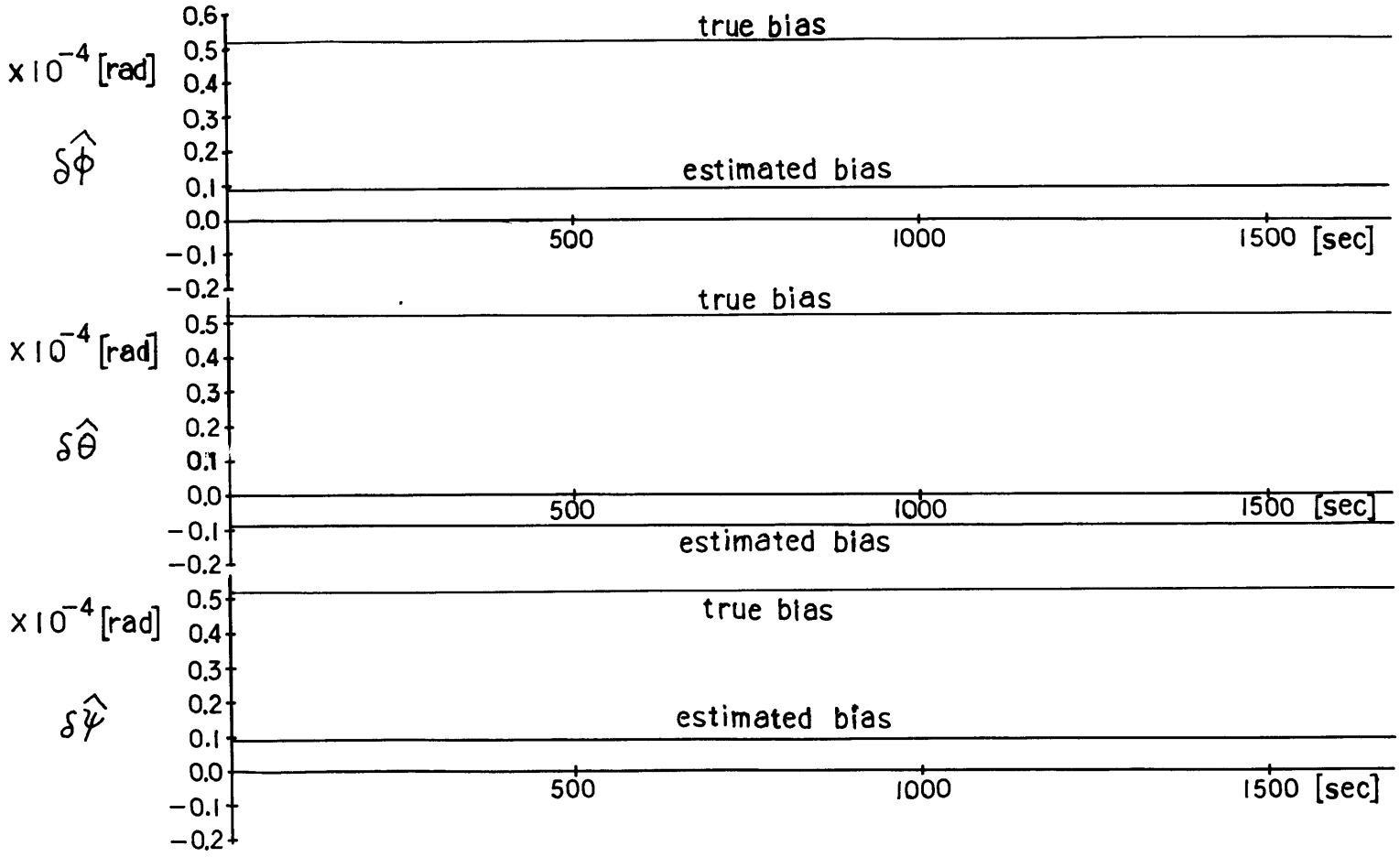

Figure 5.8 Measurement Bias Estimates

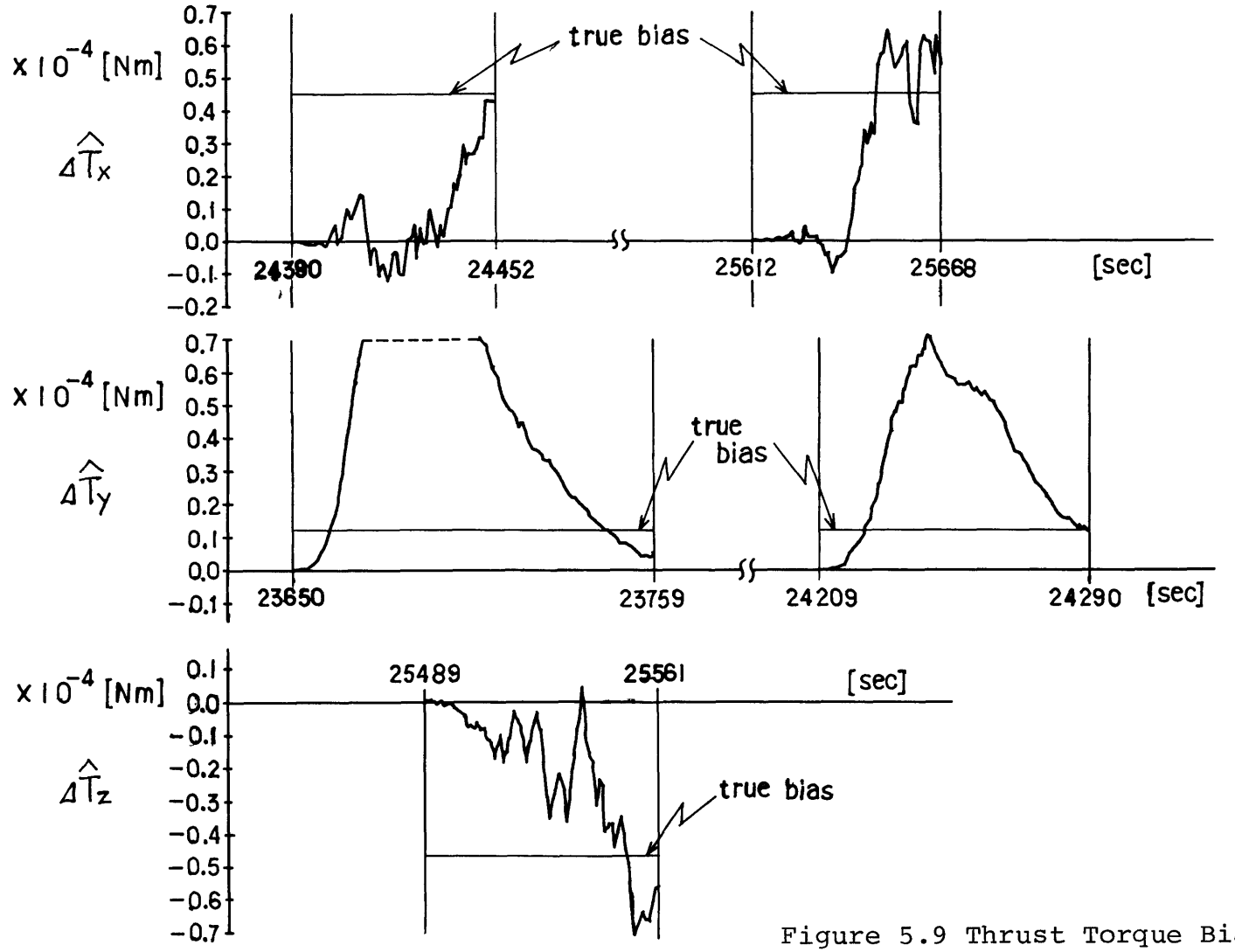

Figure 5.9 Thrust Torque Bias Estimates

CHAPTER 6

DISCUSSION OF RESULTS

First of all, the auther would like to express his satisfaction about the excellent estimates of the solar pressure torque biases shown in Fig. 5.7. These results give us assurance that our control scheme is basically feasible for practical use.

Fig. 5.2 yields closely optimal trajectories which show that the real-time control law works very well. The limit cycle period is about 1200 seconds (20 minutes), and the margins to the angle limits are $0.0 \sim 0.06 \times 10^{-3}$ [rad] for the thrusting trajectories and $0.04 \sim 0.18 \times 10^{-3}$ [rad] for the thrust-free trajectories. These deviations are equal to $0 \sim 3.4\%$ and $2.3 \sim 10\%$ of the magnitude of the limit angle window respectively. M. H. Kaplan suggested an effective total margin of 35%[7] in his conventional control scheme. Then our results are significantly closer to the optimal trajectory. There are two factors which prevent zero-margin — angle and angle rate estimation errors, and finite sampling period. Fig. 5.3 shows well behaved estimation errors. However, a small estimation error in the angle rate contributes much to the prediction error of a thrust-free trajectory.

For example, the angle rate estimation error of 0.01×10^{-5} [rad/sec] creates the angle prediction error of 0.06×10^{-3} [rad] for a thrust-free trajectory whereas it creates only 0.003×10^{-3} [rad] for a thrusting trajectory. Both prediction errors are at the point where each trajectory is closest to the corresponding angle limit. Therefore, the accuracy of the state estimates at the points where the thruster is to be turned on or off is the most critical factor in this control scheme.

The finite sampling period creates the same problem. The state transition during a sampling interval just before thrust-on/off takes place becomes $\{ 0.005 \times 10^{-3}$ [rad], 0.022×10^{-5} [rad/sec] $\}$ for a thrusting trajectory and $\{ 0.005 \times 10^{-3}$ [rad], 0.001×10^{-5} [rad/sec] $\}$ for a thrust-free trajectory. The resulting change in the maximum excursion of the predicted trajectory, for each sampling period, is then 0.137×10^{-3} [rad] for a thrust-free trajectory and 0.0053×10^{-3} [rad] for a thrusting trajectory. This defines the basic limit of resolution for the controlled angle margin.

Fig. 5.4 shows these facts more clearly. The pitch axis has smaller moment of inertia; 1/5 of that of the roll axis, and smaller thrusting torque; 1/4 fo that of the roll axis. Then the pitch state moves faster than the roll state. Actually the variations of the margins during one sampling interval are about 0.22×10^{-3} [rad] for a thrusting trajectory and about 0.07×10^{-3} [rad] for a thrust-free trajectory.

Therefore, the large margins of the thrusting trajectories are mainly caused by the relatively larger sampling interval of the thrust-free trajectory. However, the large margins of the thrust-free trajectories are mainly due to the state estimation errors. Fig. 5.5 shows that fact. The pitch angle rate estimation errors are far larger than that of the roll angle rate while the other estimation errors have the same order. The reason for this discrepancy is seen in Fig. 5.9 which shows very large estimation errors in the pitch thrusting torque bias. This is the direct cause of the large pitch angle rate estimation errors. In addition to the higher acceleration due to the smaller moment of inertia, the initial bias variance of $\Delta\hat{T}y$ was set relatively larger than for the other axes; thus the estimate responded sharply.

Fig. 5.4 shows another problem. The pitch axis is more sensitive to coupling torque from thrusting in the other axes, and this might lead to a violation of the limit angle. To avoid this problem, three dimensional prediction equations would be needed. However, adopting a bilateral thrusting scheme, in which the controller calls for torque in the same sense as the estimated external disturbance torque if the angle limit is about to be violated, is sufficient and easier to implement operationally. We can see the limitation of our prediction equations through the thrust-free trajectory of the yaw state in Fig. 5.6. It clearly represents accumulated prediction errors since the time span of the trajectory is 4000 sec (67 min.).

In this case bilateral thrusting is the best practical way of avoiding the violation.

Fig. 5.8 shows the measurement bias estimations. The bias estimates are almost constant after the first correction for the entire time region under consideration here. However, the measurement bias correction gains do not become insensitive significantly; rather, they maintain meaningful values. This means that the estimation process is still working and more time is needed to make these biases clearly observable.

The thrusting torque bias estimations are presented in Fig. 5.9. These biases are fairly well estimated. In this simulation these estimations are performed quite separately in each thrusting period. That is, the initial estimates are always set to zero and the bias variances are set to values proportional to the nominal thrusting torque level which implies no previous input of information. The covariances of the bias estimate with other estimated variables was initialized at zero. Then the estimates repeat the same process each time. Since the actual torque levels are assumed constants, the continuation of the estimation process over each thrusting phase would give us better and more stable estimates. And if so, the measurement bias estimates might be improved slightly because some part of the bias free residuals would contribute to the measurement bias corrections. Certainly the estimates of the prime states would be improved and thus the spacecraft trajectories would approach the specified error limits more closely.

So far we have reviewed the simulation results. Those results are sufficient to give us confidence that this control scheme can be applied in an actual system. Although there are some problems to be solved before practical implementation, the author believes that most of the problems can be solved operationally. This means no theoretical modification is expected to be required.

CHAPTER 7

CONCLUSION

This research was motivated by the demand that more accurate and efficient attitude control schemes should be developed to support the increasingly sophisticated missions required of geo-synchronous satellites.

A simple and accurate attitude control system could potentialy be realized by an all-electric thruster three-axes attitude control satellite. However, this control system has some disadvantages such as higher fuel and power consumptions, and frequent interruptions to the mission due the effects of thrusting.

The author has proposed an optimal control scheme which not only satisfies the accuracy requirements but also conserves fuel and power, and reduces the interruptions. This scheme achieves the maximum period soft-limit cycle which is possible only when the solar pressure torque, which is the major disturbance torque, is estimated. For the reason of numerical advantages, the 'Separate-Bias' Kalman filter was used to estimate the prime state and the biases.

The simulation results showed feasibility and very good performance of this control scheme. Especially the solar pressure torque bias was estimated very accurately. There are some detailed problems to be solved for an actual implementation on a satellite. However, the author believes no major problems exist for its practical application.

APPENDIX A

Definitions of Coefficient Matrics of the Discrete-Time State Difference Equation

$$Ad = \begin{bmatrix} 1-2w_0^2aT^2 & 0 & 0 & T+\frac{1}{6}w_0^2(C+\nu)T^3 & 0 & \frac{1}{2}w_0(1-a)T^2 \\ 0 & 1-\frac{3}{2}w_0^2bT^2 & 0 & 0 & T-\frac{1}{3}w_0^2bT^3 & 0 \\ 0 & 0 & 1-\frac{1}{2}w_0^2cT^2 & \frac{1}{2}w_0(C-1)T^2 & 0 & T+\frac{1}{6}w_0^2(4a+\nu)T^3 \\ -4w_0^2aT & 0 & 0 & 1+\frac{1}{2}w_0^2(C+\nu)T^2 & 0 & w_0(1-a)T \\ 0 & -3w_0^2bT & 0 & 0 & 1-\frac{3}{2}w_0^2bT^2 & 0 \\ 0 & 0 & -w_0^2cT & w_0(C-1)T & 0 & 1+\frac{1}{2}w_0^2(4a+\nu)T^2 \end{bmatrix}$$

$$\nu = -(3a+ac+1)$$

$$Bd = \begin{bmatrix} \frac{1}{I_x}\left\{\frac{1}{2}T^2-\frac{1}{96}w_0^2\frac{1}{a}(C\nu+\nu^2-4aC)T^4\right\} & 0 \\ 0 & \frac{1}{I_y}\left\{\frac{1}{2}T^2-\frac{1}{8}w_0^2bT^4\right\} \\ \frac{1}{I_x}\left\{\frac{1}{6}w_0(C-1)T^3\right\} & 0 \\ \frac{1}{I_x}\left\{T+\frac{1}{6}w_0^2(C+\nu)T^3\right\} & 0 \\ 0 & \frac{1}{I_y}\left\{T-\frac{1}{2}w_0^2bT^3\right\} \\ \frac{1}{I_x}\left\{\frac{1}{2}w_0(C-1)T^2\right\} & 0 \end{bmatrix}$$

$$\begin{bmatrix} \frac{1}{I_z}\left\{\frac{1}{6}w_0(1-a)T^3\right\} \\ 0 \\ \frac{1}{I_z}\left\{\frac{1}{2}T^2-\frac{1}{24}w_0^2\frac{1}{c}(4av+v^2-4ac)T^4\right\} \\ \frac{1}{I_z}\left\{\frac{1}{2}w_0(1-a)T^2\right\} \\ 0 \\ \frac{1}{I_z}\left\{T+\frac{1}{6}w_0^2(4a+v)T^3\right\} \end{bmatrix}$$

$$Cd(i)=\begin{bmatrix} -\frac{\sin w_0t_i}{I_x}\left\{\frac{1}{2}T^2-\frac{1}{96}w_0^2\frac{1}{a}(cv+v^2-4ac)T^4\right\} & 0 \\ 0 & \frac{1}{I_y}\left\{\cos w_0t_i+\left(\frac{x_t}{z_t}\right)\sin w_0t_i\right\}\left\{\frac{1}{2}T^2-\frac{1}{8}w_0^2bT^4\right\} \\ -\frac{\sin w_0t_i}{I_x}\left\{\frac{1}{6}w_0(c-1)T^3\right\} & 0 \\ -\frac{\sin w_0t_i}{I_x}\left\{T+\frac{1}{6}w_0^2(c+v)T^3\right\} & 0 \\ 0 & \frac{1}{I_y}\left\{\cos w_0t_i+\left(\frac{x_t}{z_t}\right)\sin w_0t_i\right\}\left\{T-\frac{1}{2}w_0^2bT^3\right\} \\ -\frac{\sin w_0t_i}{I_x}\left\{\frac{1}{2}w_0(c-1)T^2\right\} & 0 \end{bmatrix}$$

$$\left[\begin{array}{cc} -\frac{\cos w_0t_i}{I_z}\left\{\frac{1}{6}w_0(1-a)T^3\right\} & -\frac{1}{I_x}\left\{\frac{1}{2}T^2-\frac{1}{96}w_0^2\frac{1}{a}(cv+v^2-4ac)T^4\right\} \\ 0 & 0 \\ -\frac{\cos w_0t_i}{I_z}\left\{\frac{1}{2}T^2-\frac{1}{24}w_0^2\frac{1}{c}(4av+v^2-4ac)T^4\right\} & -\frac{1}{I_x}\left\{\frac{1}{6}w_0(c-1)T^3\right\} \\ -\frac{\cos w_0t_i}{I_z}\left\{\frac{1}{2}w_0(1-a)T^2\right\} & -\frac{1}{I_x}\left\{T+\frac{1}{6}w_0^2(c+v)T^3\right\} \\ 0 & 0 \\ -\frac{\cos w_0t_i}{I_z}\left\{T+\frac{1}{6}w_0^2(4a+v)T^3\right\} & -\frac{1}{I_x}\left\{\frac{1}{2}w_0(c-1)T^2\right\} \end{array}\right.$$

$$\left[\begin{array}{cc|ccc} 0 & -\frac{1}{I_z}\left\{\frac{1}{6}w_0(1-a)T^3\right\} & 0 & 0 & 0 \\ -\frac{1}{I_y}\left\{\frac{1}{2}T^2-\frac{1}{8}w_0^2bT^4\right\} & 0 & 0 & 0 & 0 \\ 0 & -\frac{1}{I_z}\left\{\frac{1}{2}T^2-\frac{1}{24}w_0^2\frac{1}{c}(4av+v^2-4ac)T^4\right\} & 0 & 0 & 0 \\ 0 & -\frac{1}{I_z}\left\{\frac{1}{2}w_0(1-a)T^2\right\} & 0 & 0 & 0 \\ -\frac{1}{I_y}\left\{T-\frac{1}{2}w_0^2bT^3\right\} & 0 & 0 & 0 & 0 \\ 0 & -\frac{1}{I_z}\left\{T+\frac{1}{6}w_0^2(4a+v)T^3\right\} & 0 & 0 & 0 \end{array}\right]$$

$$\nabla t(i) = \int_0^T e^{A\tau'} B \nabla t B^T e^{A^T\tau'} d\tau'$$

$$= \begin{bmatrix}
\frac{1}{3}\sigma_1 T^3 + w_0^2\{\frac{1}{15}\sigma_1(C+\nu) + \frac{1}{20}\sigma_3(1-a)^2\}T^5 & 0 \\
0 & \frac{1}{3}\sigma_2 T^3 - \frac{2}{15}w_0^2\sigma_2 b T^5 \\
\frac{1}{8}w_0\{\sigma_1(C-1) + \sigma_3(1-a)\}T^4 & 0 \\
\frac{1}{2}\sigma_1 T^2 + w_0^2\{\frac{1}{6}\sigma_1(C+\nu) + \frac{1}{8}\sigma_3(1-a)^2\}T^4 & 0 \\
0 & \frac{1}{2}\sigma_2 T^2 - \frac{11}{24}w_0^2\sigma_2 b T^4 \\
w_0\{\frac{1}{3}\sigma_1(C-1) + \frac{1}{6}\sigma_3(1-a)\}T^3 & 0
\end{bmatrix}$$

$$\begin{bmatrix}
\frac{1}{8}w_0\{\sigma_1(C-1) + \sigma_3(1-a)\}T^4 & \frac{1}{2}\sigma_1 T^2 + w_0^2\{\frac{1}{6}\sigma_1(C+\nu) + \frac{1}{8}\sigma_3(1-a)^2\}T^4 \\
0 & 0 \\
\frac{1}{3}\sigma_3 T^3 + w_0^2\{\frac{1}{20}\sigma_1(C-1)^2 + \frac{1}{15}\sigma_3(4a+\nu)\}T^5 & w_0\{\frac{1}{6}\sigma_1(C-1) + \frac{1}{3}\sigma_3(1-a)\}T^3 \\
w_0\{\frac{1}{6}\sigma_1(C-1) + \frac{1}{3}\sigma_3(1-a)\}T^3 & \sigma_1 T + w_0^2\{\frac{1}{3}\sigma_1(C+\nu) + \frac{1}{3}\sigma_3(1-a)^2\}T^3 \\
0 & 0 \\
\frac{1}{2}\sigma_3 T^2 + w_0^2\{\frac{1}{8}\sigma_1(C-1)^2 + \frac{1}{6}\sigma_3(4a+\nu)\}T^4 & w_0\{\frac{1}{2}\sigma_1(C-1) + \frac{1}{2}\sigma_3(1-a)\}T^2
\end{bmatrix}$$

$$\begin{bmatrix}
0 & w_0\{\frac{1}{3}\sigma_1(C-1) + \frac{1}{6}\sigma_3(1-a)\}T^3 \\
\frac{1}{2}\sigma_2 T^2 - \frac{11}{24}w_0^2\sigma_2 b T^4 & 0 \\
0 & \frac{1}{2}\sigma_3 T^2 + w_0^2\{\frac{1}{8}\sigma_1(C-1)^2 + \frac{1}{6}\sigma_3(4a+\nu)\}T^4 \\
0 & w_0\{\frac{1}{2}\sigma_1(C-1) + \frac{1}{2}\sigma_3(1-a)\}T^2 \\
\sigma_2 T - w_0^2\sigma_2 b T^3 & 0 \\
0 & \sigma_3 T + w_0^3\{\frac{1}{3}\sigma_1(C-1)^2 + \frac{1}{3}\sigma_3(4a+\nu)\}T^3
\end{bmatrix}$$

where

$$\sigma_1 = \sigma_{t1}^2\left(\frac{1}{I_x}\right)^2$$

$$\sigma_2 = \sigma_{t2}^2\left(\frac{1}{I_y}\right)^2$$

$$\sigma_3 = \sigma_{t3}^2\left(\frac{1}{I_z}\right)^2$$

REFERENCES

1. Martin, J., Communications Satellite Systems, Prentice-Hall, 1978.

2. Kaplan, M.H., "All-Electric Thruster Control of a Geostationary Communications Satellite", Journal of Spacecraft and Rockets, Vol. 10, Feb. 1973.

3. Kaplan, M.H., "Design and Operational Aspects of All-Electric Thruster Control Systems for Geostationary Satellites", Journal of Spacecraft and Rockets, Vol. 12, Nov. 1975.

4. Gelb, A., Applied Optimal Estimation, M.I.T.Press, 1974. pp. 78-84.

5. Friedland, B., "Treatment of Bias in Recursive Filtering", IEEE-Automatic Control, Vol. AC-14, Aug. 1969.

6. Kaplan, M.H., Modern Spacecraft Dynamics and Control, Wiley, 1976. pp 49-50 and pp. 262-265.

7. Sutton, G.P., and Ross, D.M., Rocket Propulsion Elements, 4th Edition, John Wiley and Sons, 1976. Chapter 13.

8. Kwakernaak, H., and Sivan, R., Linear Optimal Control Systems, Wiley-Interscience, 1972. pp. 100-103.

9. Jazwinski, A.H., Stochastic Processes and Filtering Theory, Academic Press, 1970. pp. 81-85.